NASA Contractor Report 177523

Enhancements to a New Free Wake Hover Analysis

Todd R. Quackenbush
Daniel A. Wachspress

Continuum Dynamics, Inc., Princeton, New Jersey

Prepared for
Ames Research Center
CONTRACT NAS2–12810
April 1989

National Aeronautics and
Space Administration

Ames Research Center
Moffett Field, California 94035

TABLE OF CONTENTS

SBIR RIGHTS NOTICE
(DECEMBER 31, 1988)

The computer program described in this report contains some data that is subject to the restrictions imposed by NASA SBIR PHASE II Contract NAS2-12148. The restrictions set forth therein are applicable for a two (2)-year period effective from January 1, 1988 to December 31, 1989.

NOMENCLATURE

A	rotor disk area, ft^2
C_p	rotor power coefficient
C_T	rotor thrust coefficient
D	rotor disk diameter, ft
h_f	spacing of wake turns in the far wake, ft
K	coefficient of induced component of total power
p	pressure, psf
$\vec{q}$	vector of crossflow velocities at wake collocation points, ft/sec
Q	influence coefficient submatrices
r	radial distance from rotor hub, ft
T	rotor thrust, lb
w	magnitude of flow velocity in the rotor wake, ft/sec
$\vec{w}$	vector of downwash velocities at blade control points, ft/sec
$\Delta\vec{x}$	vector of wake collocation point position perturbations, ft
z	vertical height of rotor hub or of vortex wake turns above ground, ft
$\Delta\vec{\gamma}$	vector of blade quadrilateral bound circulation perturbations, ft^2/sec
Γ	circulation strength of the tip vortex, ft^2/sec
Ω	rotor rotation rate, rad/sec

1. INTRODUCTION

Recent research in free wake analysis of hovering rotors has led to the development of a new approach to this problem. References 1 and 2 document the development of a relaxation solution method for the wake geometry of a hovering rotor that bypasses the convergence difficulties associated with previous free wake models based on Lagrangian time stepping (see, for example, Refs. 3 and 4). As will be described briefly below, this new analysis employs an influence coefficient formulation to solve directly for the wake geometry and bound circulation distribution on the rotor blades that satisfy the correct physical boundary conditions on the blade and in the wake (i.e., flow tangency at selected control points on the blade and zero crossflow velocity at collocation points in the wake). References 5 and 6 illustrate the success of this new method (which has been incorporated into a computer code dubbed EHPIC - Evaluation of Hover Performance using Influence Coefficients) in predicting the performance of a wide variety of rotor configurations.

Subsequent to the development of the original version of EHPIC, it was resolved to undertake several enhancements to the basic code that could take advantage of latent capabilities in the analysis and which would considerably enhance the computational efficiency of the procedure. First, as will be described in more detail below, the basic version of EHPIC described in Reference 2 is applicable only to rotors operating out of ground effect. It is in general possible to simulate the presence of a ground plane in an inviscid flow with embedded vorticity through the use of an image system located symmetrically with respect to the ground. Following a brief review of the basic principles of the influence coefficient solution method in Section 2, Section 3 below presents a discussion of the implementation of an image system in the baseline EHPIC code. The discussion will include an outline of the major modifications to the wake model that were undertaken for this effort as well as the results of several performance comparisons that were performed to validate the ground effect model.

The second task undertaken for this effort was prompted by another of the unique features of the influence coefficient approach. The relaxation process that takes place in the EHPIC code relies on a linearized treatment of the sensitivity of induced velocities in the wake and on the rotor blade to perturbations in the wake geometry to generate a converged solution for the vortex wake. As was shown in Reference 1 and as will be discussed further in Section 4 below, the matrix of influence coefficients that is generated as a part of this process contains information on the linear stability of the wake solution that results. Section 4 will discuss the implementation of an eigensystem analysis package that has been coupled to the upgraded EHPIC analysis to produce (at the option of the user) information on wake stability. The discussion of this topic will include an overview of the details of the solution method pertaining to the stability analysis as well as sample calculations illustrating the type of information available to the user in the new version.

Finally, in light of the considerable computational effort required to run the original version of the EHPIC analysis, it was judged appropriate to undertake an effort to improve the code's computational efficiency. For the current effort, the code itself was extensively rewritten to take advantage of the vector processing capabilities of CRAY-type supercomputers. The reprogramming effort was complicated by the intricacy of the influence coefficient evaluation process, but fundamentally standard vectorizing techniques were employed. The work on this topic will be briefly summarized in Section 5, though the bulk of the technical discussion of these modifications are contained in the updated User Manuals for the EHPIC code and in the documentation within the source code itself.

2. REVIEW OF THE EHPIC CODE

This section summarizes the technical background on the fundamentals of the influence coefficient hover analysis as implemented in the original EHPIC code. It is useful to first describe the functioning of the original hover performance analysis before proceeding with the discussion of the modifications required to include ground effect.

The general objective of a free wake hover analysis is to find the wake geometry that, for a specified rotor geometry, satisfies two conditions: first, that the wake filaments are in free motion; and second, that the flow tangency condition is satisfied on the blade. To achieve the free motion condition, the wake filament trajectories must be tangent to the local velocity vector evaluated on the filament when viewed in a rotating reference frame, i.e., there must be no cross flow velocity components at any point on the filaments under force free conditions. The coupled free wake/lifting surface hover analysis in the original EHPIC code proceeds toward this goal by first making an initial guess for the blade loads and the wake geometry. This initial guess will not, in general, satisfy the required conditions, and so must be adjusted in a succession of solution steps. To accomplish this, the independent variables in the problem (the bound circulation at stations along the blade and the vortex wake position coordinates) are systematically perturbed, and the effect of these perturbations on the dependent variables (the downwash on the blade and crossflow velocities in the wake) are summed and formed into influence coefficients. These coefficients allow the construction of a set of simultaneous linear equations in matrix form which predict the change in dependent variables due to the changes in independent variables. The coefficient array so formed can be used to null the crossflow and downwash velocities by inverting it and multiplying it by the vector of residual velocities. Were the problem purely linear, this process would yield a vector of wake displacements and circulation perturbations that would exactly null the velocities in question. In general, the process must be repeated due to the inherent nonlinearity of the problem, and only small fractions of the residual velocities are nulled in each iteration. In practice, this approach has been found to have robust convergence properties, despite the complexity of the relaxation procedure. For realistic rotor configurations with up to ten wake filaments per blade, convergence is usually achieved after ten to fifteen relaxation steps.

The individual filamentary vortices used in the wake are comprised of connected strings of Basic Curved Vortex Elements (BCVE's); these curved elements are used to generate the velocity field at all points in the flow other than on the elements themselves. For the special case of points that lie on the elements, a special treatment is used in the form of Self-Induction Vortex Elements, or SIVE's. As shown in Reference 7, the use of these curved elements substantially enhances the efficiency of modeling complex wakes and contributes materially to the high accuracy of free wake analyses. The approach taken to incorporating these effects into the original EHPIC code is described in detail in Reference 2.

A free wake analysis using such filamentary vortices necessarily involves only a finite number of turns of free vortex wake. The free wake region is composed of a number of filaments trailed from the 'primary blade'; these filaments simulate the tip vortex, inboard sheet, and root vortex of each blade. Other blades and their wakes are assumed to have a configuration identical to that of the designated primary blade, since the ideal solution will have blade-to-blade symmetry. Beyond the free wake region, the wake must be continued using a far wake model if the solution is to be physically correct. If the far wake model is poorly executed it will exert a net thrust which alters the free wake structure and interferes with the rotor. Thus, the far wake model must be as realistic and as force

free as possible. The far wake model used in the current hover analysis code is an idealized extension of the free wake. The free wake filaments are continued as ideal discrete helices into the far wake. (See Fig. 1 for a schematic of a simple tip-vortex-only case out of ground effect.) If care is taken to ensure that the far wake is attached after the wake contraction is complete, it should be very nearly force free.

At this point, it is appropriate to introduce a terminological issue. The portion of the wake model beyond the free wake has to this point been lumped into the term "far wake". However, the OGE EHPIC wake model has two distinct parts within this region. The first is directly attached to the free wake and consists of a specified number of constant-radius turns of wake whose vertical spacing is prescribed based on the dimensions of the free wake and conservation of momentum; this part, which is modeled using BCVEs, will henceforth be referred to as the "prescribed wake". When the model is run OGE, this prescribed wake is extended to infinity by using an analytical expression to sum up the effect of a semi-infinite set of helical vortex turns, each being a duplicate of the last prescribed wake turn. This part of the wake model will be referred to below as the "far wake". This analytical extension of a filament into the far wake is accomplished by approximating the curved elements as vortex particles. The velocity field of large arrays of such artifacts can be much more easily summed than that of curved vortex elements, as is discussed in Reference 7. However, such approximations are valid only if the points of evaluation are suitably distant from the element being so modeled; in general, separation distances considerably greater than the element length are required. Thus, the analytical extension is only invoked in the far wake, which has a "buffer zone" of prescribed wake (consisting of BCVEs) between it and the free wake collocation points.

With this model in place, the influence coefficient approach is able to find the physically correct, self-preserving wake geometry without the instabilities and consequent lack of convergence of earlier methods that convected the wake in a time-marching manner (Refs. 3 and 4). Furthermore, once a converged solution has been obtained, adjacent solutions that are linearly close along a performance curve are readily obtained with only a small number of relaxation steps, eliminating the need to wash out the transients that arise in time-marching schemes. This method also produces very satisfactory performance predictions for a wide range of rotors. References 5 and 6 show samples of the performance correlations achieved to date with this analysis.

One of the constraints of this solution method is that it can be applied only to systems where the desired solution is steady with respect to some reference frame. The hovering rotor out of ground effect fits in this class, because the flow can be treated as steady in a reference frame rotating with the rotor blades. Rotors in climb also qualify, and it is clear upon reflection that the hovering rotor in ground effect is also a suitable problem if an image system is used to simulate the presence of the ground plane. Even with the presence of an image system the flow remains axisymmetric and steady in the rotating frame. This observation is the starting point for the formulation of the modifications required to include ground effect ; these modifications will be described in the next section.

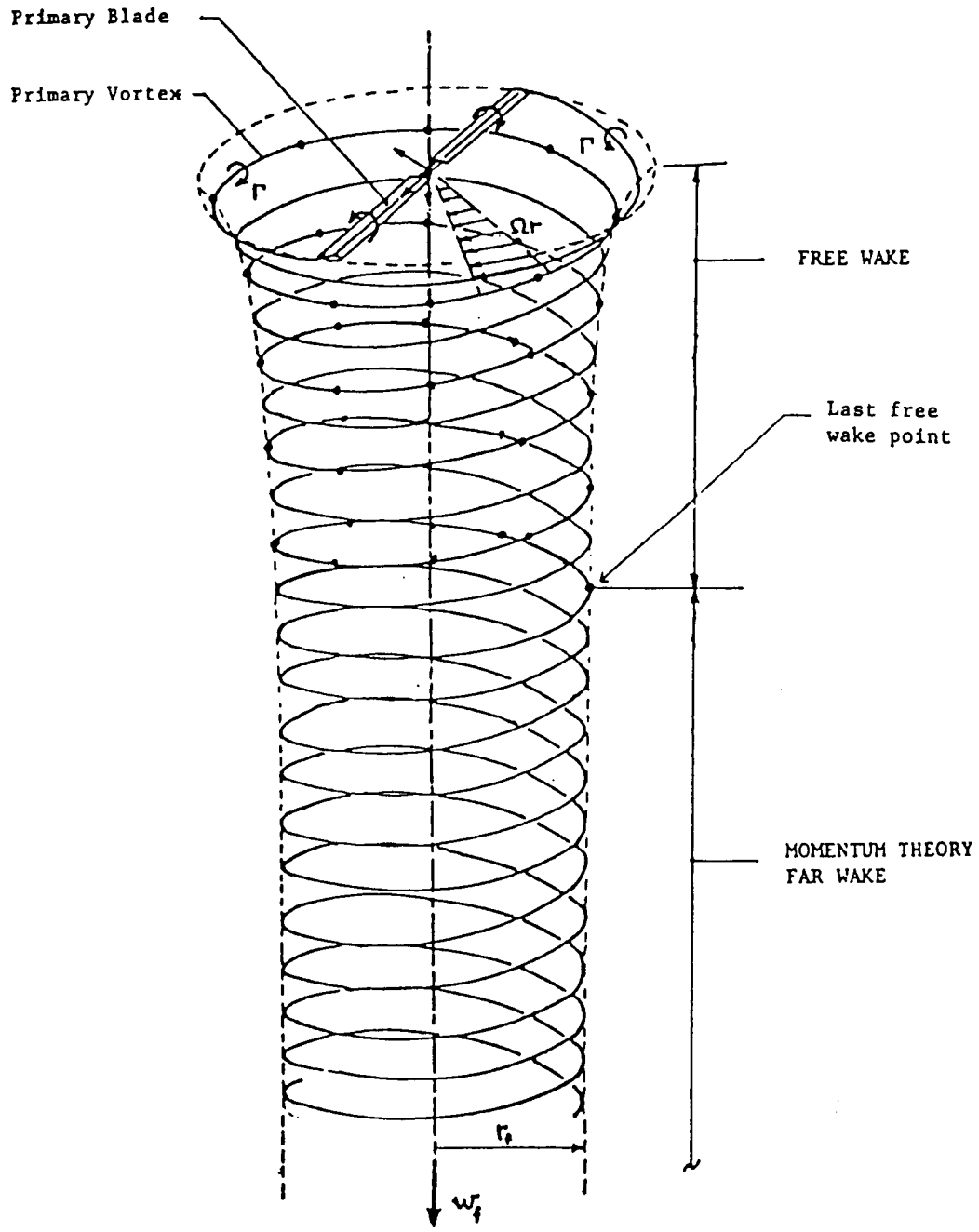

Figure 1. The two-part wake structure for the hover analysis.

3. IMPLEMENTATION OF THE GROUND PLANE MODEL

3.1 Outline of the Ground Effect Simulation

In three-dimensional, inviscid, incompressible flows with embedded vortex lines, such as the vortex wake used in the EHPIC code, it is possible, as noted above, to simulate the presence of a solid boundary by introducing an image system of the rotor and its wake. While straightforward in principle, there are a number of modeling challenges and difficulties in implementation for this type of treatment. For example, the wake model must be considerably altered for the ground effect case. The near wake model, consisting of the freely distorting free vortex filaments trailing from the each blade, undergoes relatively simple modifications. The inclusion of the image free wake 'below' the ground plane accounts for a large fraction of the effect of ground proximity. However, the treatment of the wake beyond the free wake region is still of considerable potential importance, as well, and this part of the analysis requires more substantial modifications relative to the OGE case. In addition, different approaches are required for the tip vortex, the root vortex, and the non-root inboard filaments, and each of these is now discussed in turn.

The fundamental approach to the modeling of the tip vortex is suggested by the model problem of a vortex pair approaching a solid wall. A helical vortex filament approaching a solid surface represents a nearly axisymmetric flow, and so the vortex pair model problem is instructive. The sketch in Figure 2 suggests that the pair enlarges its separation and accelerates as it approaches more and more closely to its image. This result is suggestive of the trajectory of the tip vortex as it spirals outward away from the rotor; the filament makes an asymptotic approach to the ground plane, and any given cross-section of the filament moves out radially at an increasing rate. Using an arbitrarily large extent of free wake for the tip vortex would allow this spiralling trajectory to be explicitly resolved. However, this is computationally inefficient, and is in fact unnecessary, since the tip vortex and its image nearly cancel for distant points of evaluation. Thus, it is appropriate to consider prescribed wake models that can be coupled to the free wake treatment used near the rotor. These models should conserve the major features of the actual flow field at large radial distances and should mesh smoothly with the freely distorting portion of the tip filament.

The approach taken in the modified EHPIC code is to extend the freely distorting tip vortex into the region beyond the free wake with the spacing of the filaments prescribed as a function of radial distance so that the momentum flux and mass flow within the wake will be conserved. Figure 3 gives a schematic of the prescribed wake model used; the filament spacing is based on the assumption that the flow within the wake can be described by invoking Bernoulli's equation on a streamline from a point just below the rotor disk into the far wake. (The subscripts refer to the stations indicated in Fig. 3).

$$p_2 + \frac{1}{2}\rho w_2^2 = p_3 + \frac{1}{2}\rho w_3^2 \qquad (1)$$

Other useful relationships include Bernoulli's equation between a point far above the rotor and a point at the disk, continuity at the rotor disk, and pressure equilibration in the far wake (note that the subscript 0 denotes ambient conditions):

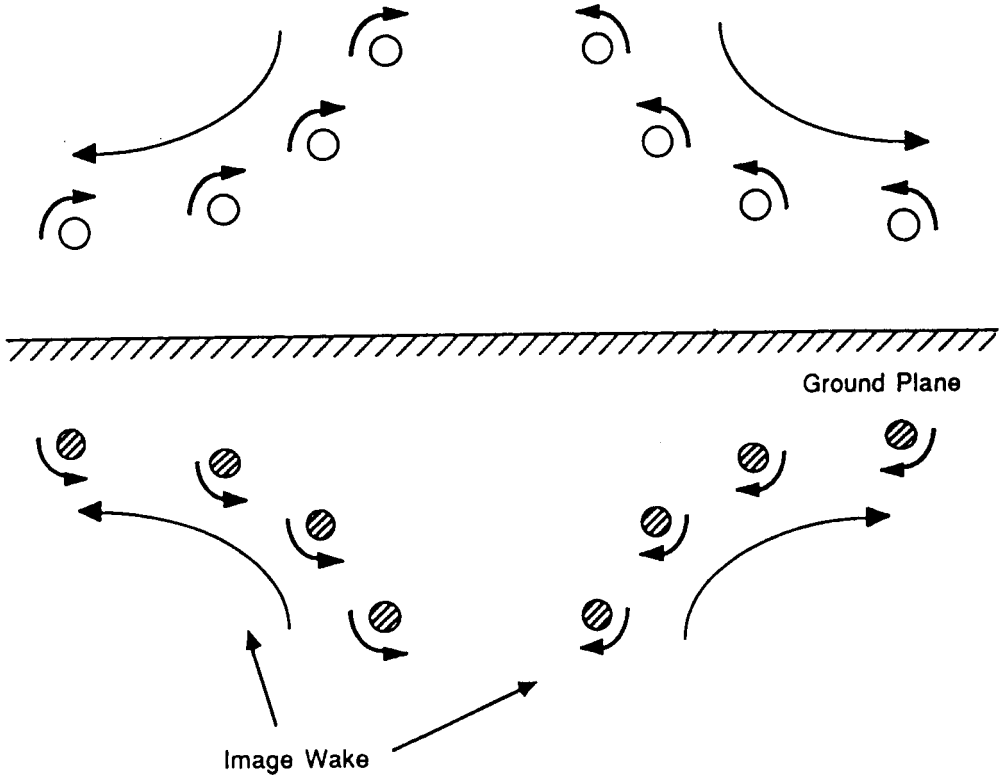

Figure 2. Schematic of a model problem for the rotor wake in ground effect: a vortex pair approaching a wall.

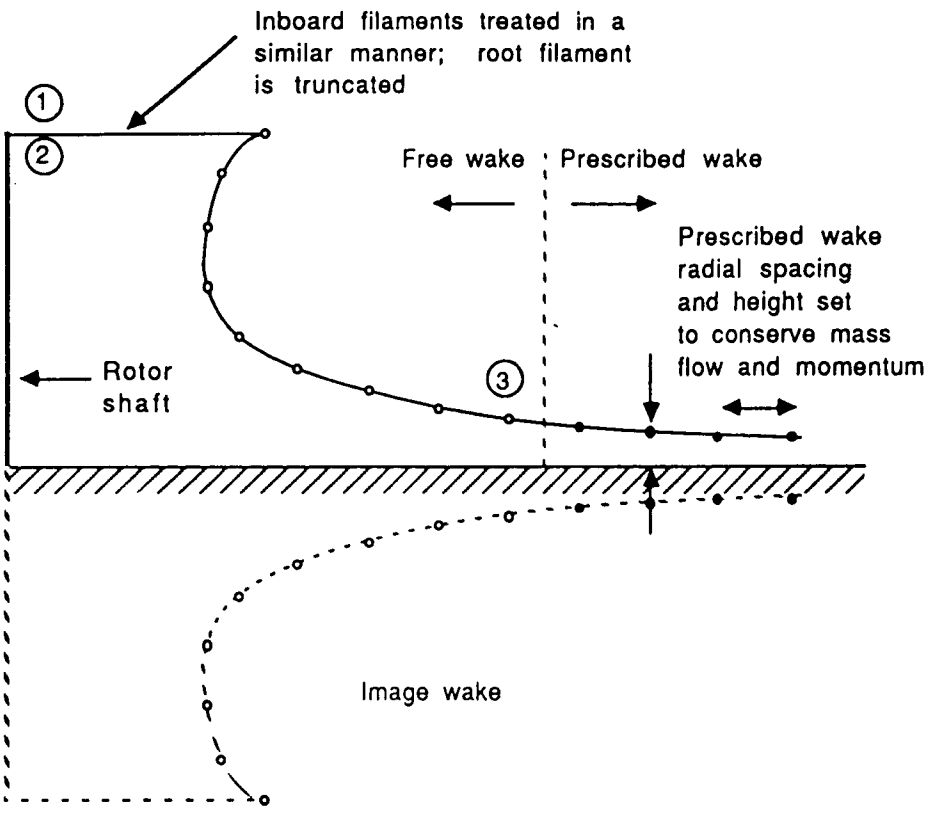

Figure 3. Schematic of a wake model in ground effect for the modified EHPIC code.

$$p_0 = p_1 + \frac{1}{2}\rho w_1^2 \tag{2}$$

$$w_1 = w_2 \tag{3}$$

$$p_0 = p_3 \tag{4}$$

Using these equations and the fact that

$$T = A(p_2 - p_1) \tag{5}$$

it can be shown that

$$w_3 = 2\sqrt{\frac{T}{2\rho A}} \tag{6}$$

This result is, of course, exactly the same as the flow velocity in the far wake for a rotor out of ground effect. For the purposes of the updated EHPIC code, the wake spacing based on this velocity is applied to prescribed wake turns at radial distances greater than one diameter from the hub. The prescribed wake location for any points lying between one radius and one diameter is obtained by interpolating the wake velocity linearly, with an assumption of zero radial velocity at r = 0. This approach assumes that the free wake region for the tip vortex of a rotor in ground effect will extend to at least one radius from the rotor hub, though the precise extent of the free wake is a function of the number of free wake turns selected by the user.

The vertical location of the prescribed wake turns is determined by applying a continuity condition based on the mass flow within the wake at the end of the free wake region. It is assumed that the mass flow passing through the cylindrical surface extending from the ground up to the last turn of free wake (station 3 in Fig. 3) remains inside the wake in the far field. Assuming incompressible flow and using the radial spacing derived just above, the vertical location of the prescribed turns of wake can be determined using the simple relationship

$$z = \frac{r_3^2 z_3}{r^2} \tag{7}$$

where the flow speed in the prescribed wake, w_3, is asssumed to be constant.

The treatment of the inboard wake in ground effect is of necessity somewhat more approximate than that of the tip vortex. The analysis of the portion of the inboard wake between the root vortex and the tip vortex is discussed below, though the treatment of the root vortex itself poses a special problem in ground effect. Experimental information shown in References 8 and 9 indicate the presence of a recirculation zone beneath the center of the rotor disk for cases in which the rotor is at or below roughly one radius in height (see Fig. 4). The influence coefficient algorithm used in the EHPIC code is applicable only to flows that are steady in the rotating reference frame. Since the actual rotor flow for IGE configurations experiences strong recirculation inboard of roughly the fifty percent radius station, it is impossible for the filamentary wake model used here to find a steady solution in this region. To capture the main features of the flow in this region, it was judged appropriate to use a prescribed helical root filament extending from the rotor disk to a height near the ground. Given the sign of the vorticity trailing from the blade root, this model of the inboard wake will set up a flow with the correct overall pattern.

Further discussion of experimental information on flow beneath a lifting rotor in ground effect can be found in Fradenburgh (Ref. 10), which also points out the existence of this recirculation region. This 'dead zone' of relatively low velocity, recirculating flow and essentially constant pressure lies in a roughly conical region, extending out to approximately 0.5 rotor radii, as seen in Fig 4. Judging from the available experimental evidence, there appears to be a dividing streamline that forms the border between the flow that is drawn through the rotor out into the far field and that which recirculates in the vicinity of the rotor shaft. The role of the root filament in the current ground effect model is, as noted above, to generate the interior recirculation; the role of the other inboard filaments, in conjunction with the tip vortex, is to model the exterior flow that passes through the rotor and out into the far field. Both the tip and inboard filaments are currently modeled using several turns of free wake followed by a prescribed wake region; the tip vortex prescribed wake is assumed to move at half the far wake flow speed, w_3, while the inboard filaments experience the full level of w_3 (a treatment analogous to the hover wake).

Currently, each tip vortex filament is terminated at the end of the prescribed wake. This, of course, introuduces some error into the downwash computed at the rotor disk, and an analytical study was undertaken to quantify this error. The effect of the far wake of the tip vortex (and its image) was computed by calculating the total effect of two concentric annular sheets of vorticity, each with an average strength based on the estimated circulation and spacing of the tip vortex in the far wake; the sheet strength is in fact equal to the far wake velocity given in Equation 6. A schematic of the analytical model used is shown in Figure 5. This figure shows a cut through what is, of course, an axisymmetric flow field. The two sheets were assumed to be fixed a specified distance above and below the ground plane and were also assumed to contain oppposite-sign vorticity so that they could model the contribution of the truncated far wake and its image on the rotor disk. Clearly, the contributions of the companion annular sheets will cancel for points of evaluation whose distance from the sheets is large compared to the spacing between them.

This model is obviously a simplified representation of the actual far wake. The intent in invoking it was to provide order-of-magnitude values for the downwash contributed by the far wake which could in turn be used to formulate rules of thumb for specifying the extent of free wake that should typically be used. The downwash was estimated by integrating the Biot-Savart law contributions from each annular slice of the far wake sheets to the velocity at points near the center of the rotor disk. Using this model, it was estimated that for typical cases the error in downwash at the rotor disk could be kept to no more than two percent of the level predicted by simple momentum theory if the

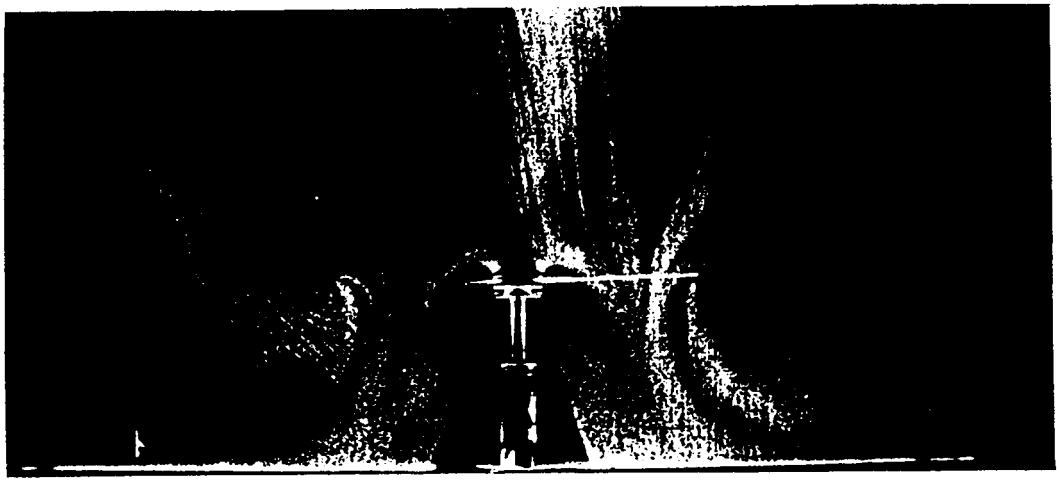

Figure 4a. Flow visualization for a model rotor at z/D = 0.5 (from Ref. 9).

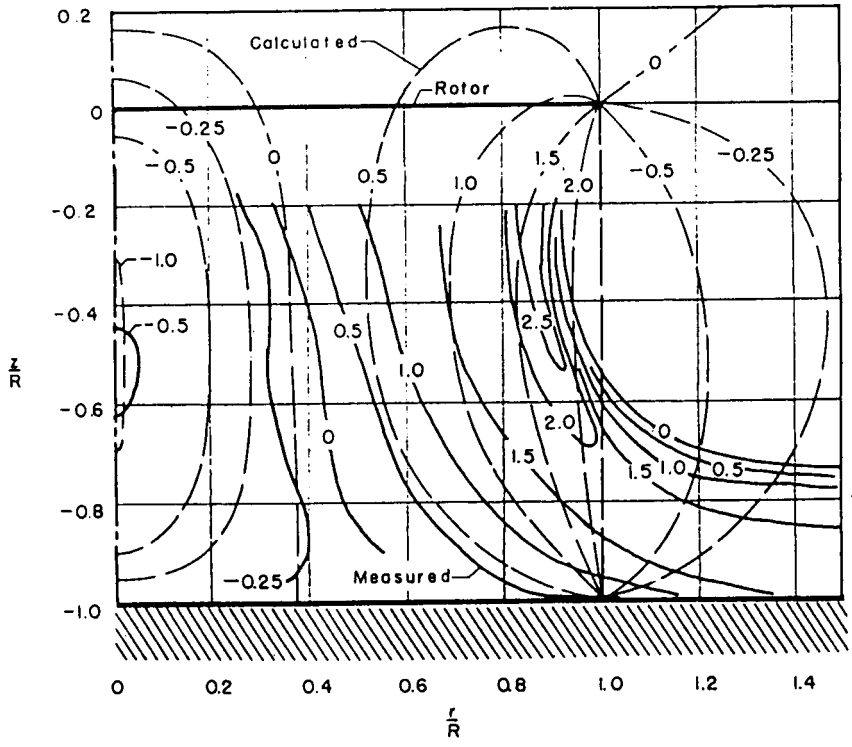

Figure 4b. Comparison of measured induced velocity contours to calculations using simple vortex theory (for the rotor of Figure 4a using the theory of Ref. 9).

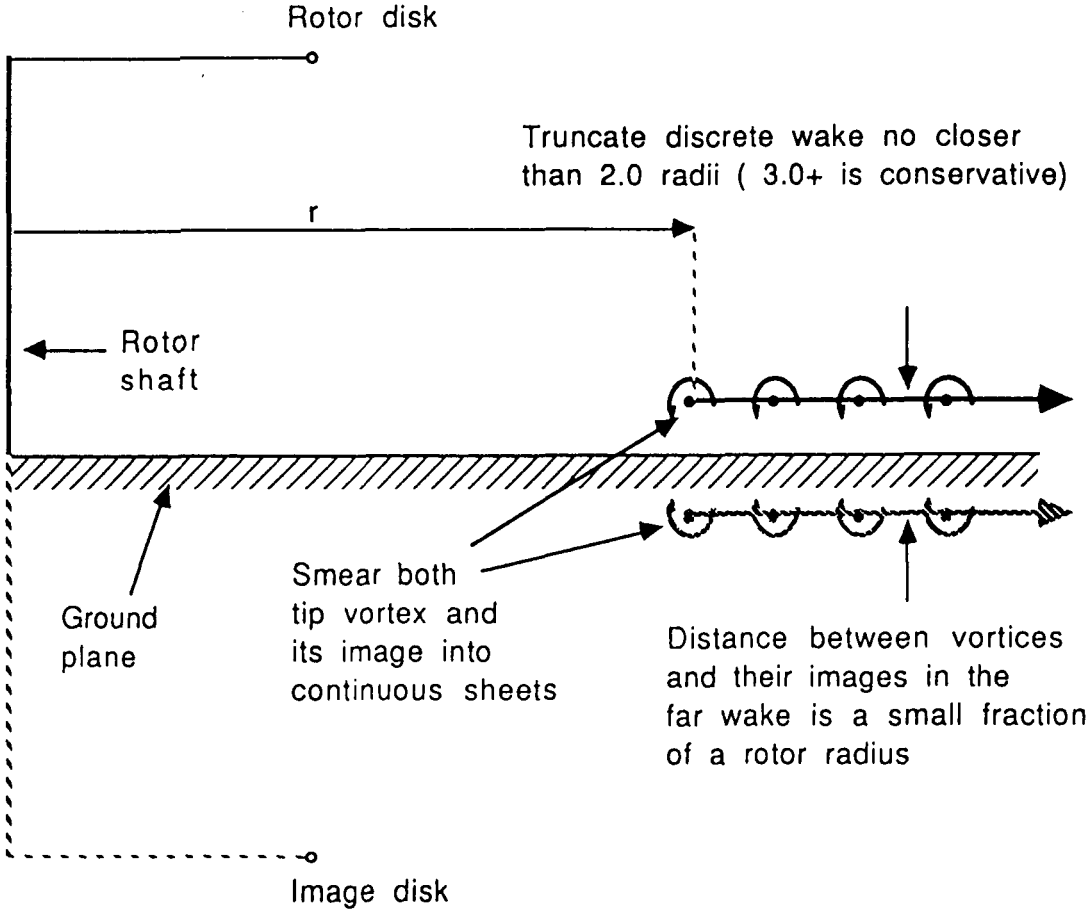

Figure 5. Model used to compute effect of the discrete far wake and its image on the rotor disk; the two configurations largely cancel for points of evaluation far away.

truncation of the wake was carried out no closer than one rotor diameter from the shaft. This estimate does not include the additional cancellation that arises due to the entrainment of opposite-sign vorticity from the inboard wake or from the ground boundary layer.

A conservative approach to the selection of wake length, then, would be to extend the tip vortex wake out to beyond one rotor diameter (closer to two diameters if possible) and in all cases to have the radial extent of wake at least equal to the rotor height. The selection of wake length for the inboard filaments is somewhat less critical, since they effectively cancel with their images even faster than the tip vortices. Experience to date indicates that reasonable, well-behaved solutions are achieved by using roughly half the number of wake turns assigned to the tip vortex; an even smaller ratio (inboard/tip) is often appropriate for cases very close to the ground. With these criteria in place, the accuracy achieved was judged to be acceptable for current purposes.

Another difference between the OGE and IGE versions of EHPIC Mod 1.0 is the initial relaxation used within the influence coefficient scheme. To achieve reliable convergence, it is advantageous to relax slowly away from a known solution in the initial portions of the calculation. For OGE cases, the computation is started by imposing an 'artificial climb' velocity on the rotor and nulling the strength of all the vortex trailers by bypassing the imposition of flow tangency on the blade; the climb velocity is slowly decreased and the flow tangency condition is gradually phased in so as to allow smooth convergence to the final free wake solution. The magnitude of the initial climb velocity is scaled by a user-defined parameter, CTINIT. In ground effect, a different baseline model is used in place of the uniform stream associated with 'artificial climb'; computations executed IGE begin with the rotor immersed in a stagnation point flow whose initial magnitude is also scaled by CTINIT and which phases out in a gradual fashion. As discussed below, however, the proper choice for CTINIT for IGE cases differs from the level that is appropriate for OGE calculations.

The behavior of rotor wakes in ground effect is illustrated in Figures 6-11, which show converged wake geometries for a four-bladed OH-6 rotor system operating in ground effect at heights from z/D = 0.4 to 2.0. Four trailing filaments are used in these sample cases. The tip filament employs at least three turns of free wake and between one and two turns of prescribed wake. The next two inboard filaments use roughly half as much free wake while retaining the same amount of prescribed wake. The root filament trajectory is prescribed, though its pitch adapts to the current value of thrust on the rotor. Note that in most cases the tip filament and the free inboard filaments merge smoothly into the far wake.

3.2 Limitations of the Current Ground Effect Treatment

The discussion to this point has mentioned the limitations of the current ground effect model only in passing. It is important to have the approximations that figure in this model clearly in mind when interpreting the results of the calculation of loads and wake geometry.

First, this is an inviscid model that neglects any effect of the ground boundary layer on the evolution of the wake. The effect of imposing a no-slip boundary condition on the ground, in general, leads to the generation of opposite-sign vorticity that merges with the organized flow of the vortex wake and causes it to diffuse rapidly. The truncation of the far wake of the inboard and tip filaments is clearly only an approximate treatment of this process, one whose adequacy is difficult to judge except by its effect on the integrated performance comparisons that are discussed in the next section.

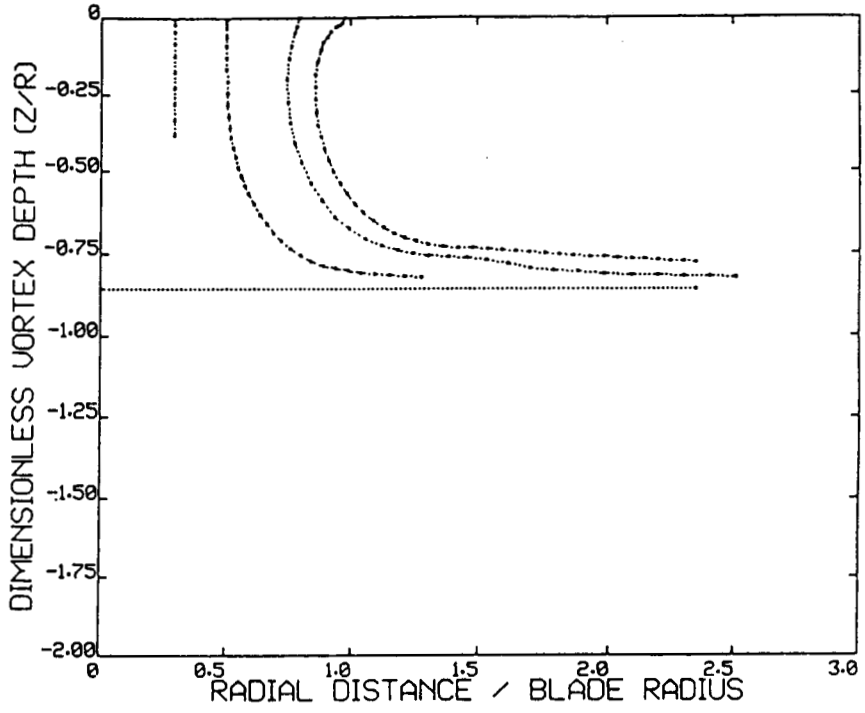

Figure 6. Wake geometry for OH-6 at z/D = .430 .

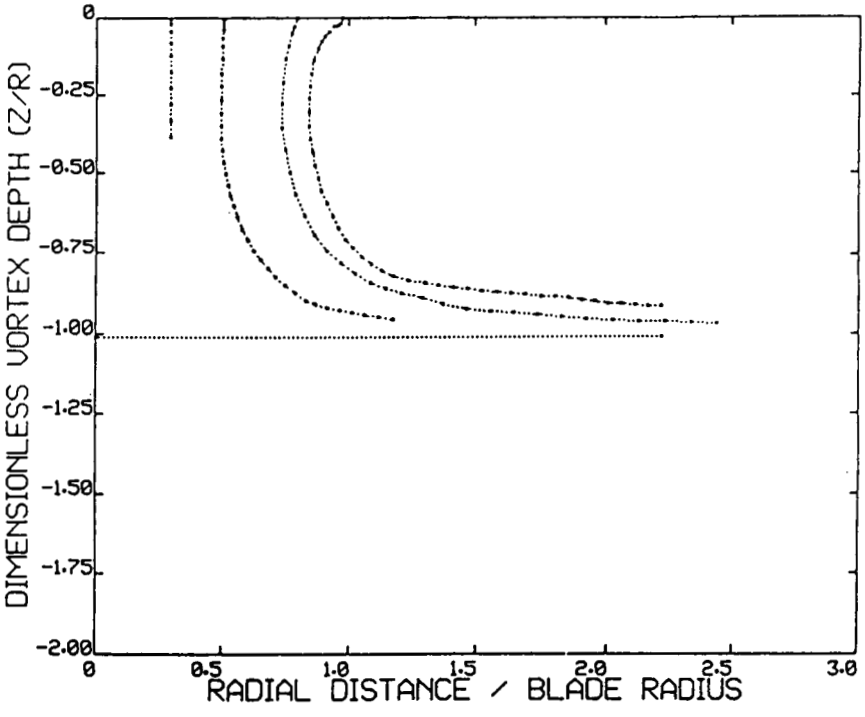

Figure 7. Wake geometry for OH-6 at z/D = .506 .

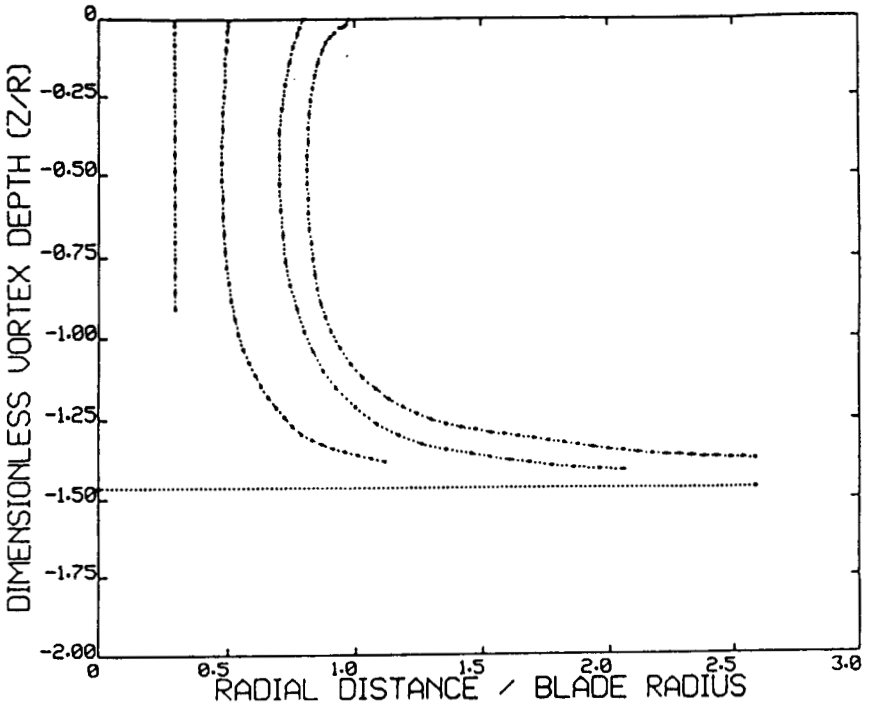

Figure 8. Wake geometry for OH-6 at z/D = .734 .

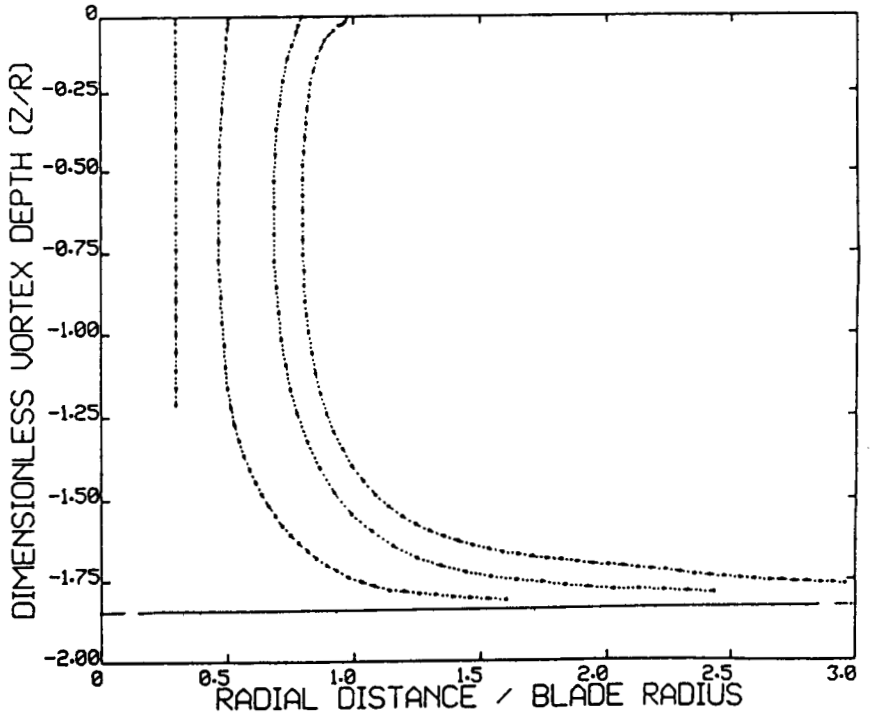

Figure 9. Wake geometry for OH-6 at z/D = .924 .

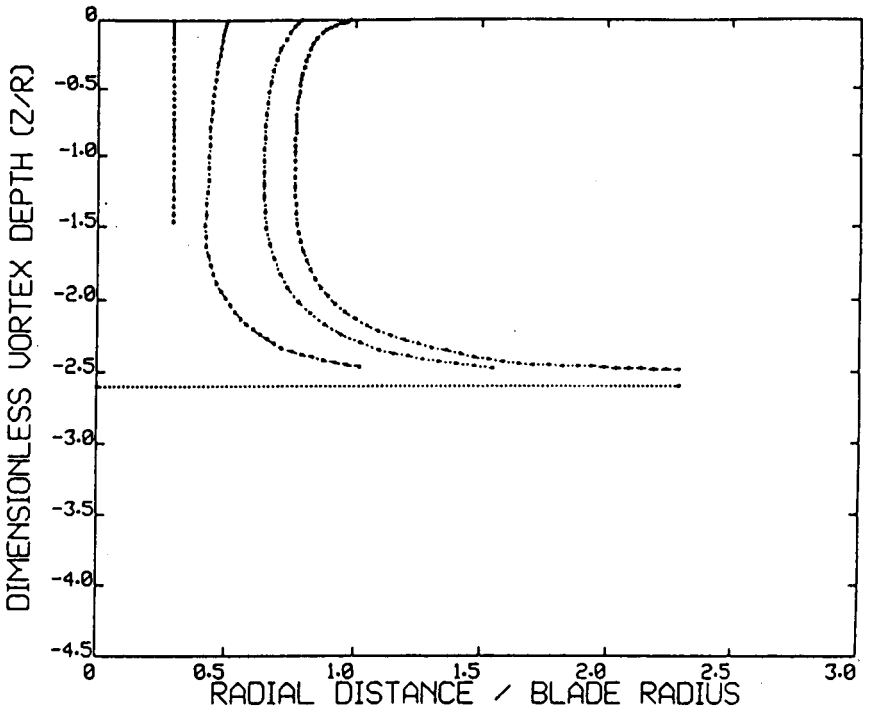

Figure 10. Wake geometry for OH-6 at z/D = 1.303 .

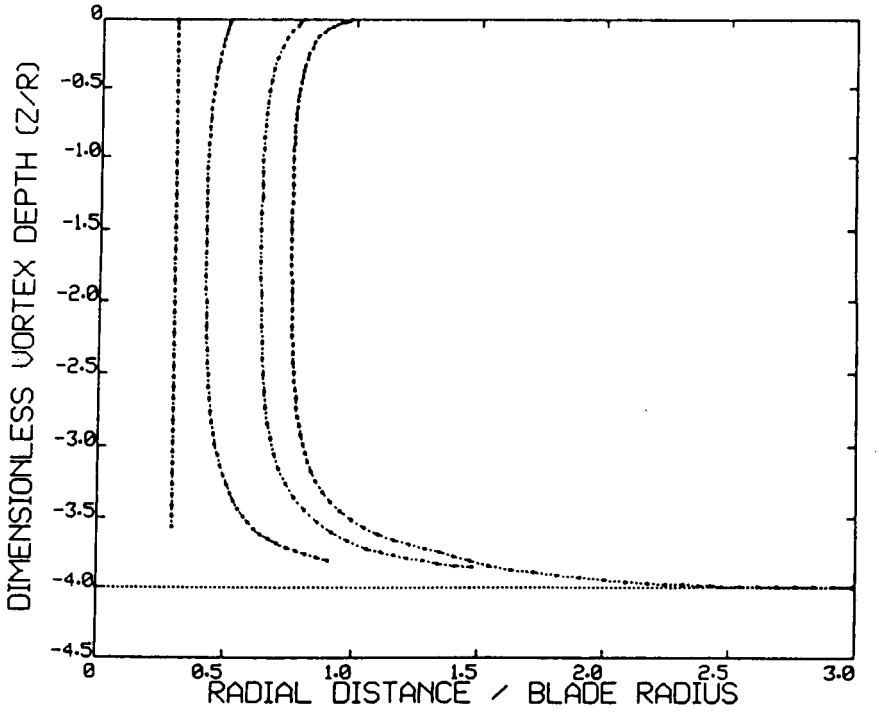

Figure 11. Wake geometry for OH-6 at z/D = 2.0 .

A second and related point is that the computations carried out with the EHPIC code solve for a steady flow field which is assumed to generate the same mean loads on the rotor as the actual unsteady flow field that exists in the vicinity of a lifting rotor. The persistent unsteadiness of rotor flow fields is a phenomenon that is well substantiated experimentally (Ref. 11); it manifests itself in the form of the progressive breakdown of the discrete filamentary tip vortices, a breakdown that culminates in the generation of a flow resembling a turbulent jet beneath rotors operating out of ground effect. The proximity of the ground may well accelerate the development of these instabilities, so it is likely that the effect of unsteadiness in the rotor flow field is at least as important for rotors operating IGE as it is for OGE rotors. The same assumption applies for IGE calculations using EHPIC as did for the OGE results discussed in References 1, 2, 5, and 6, i.e., that by tracking the free evolution of filamentary vortices that correctly preserve the strength and centroids of the vorticity trailed from the blade an accurate computation of the mean flow field surrounding the rotor can be accomplished.

Finally, it has been found that selecting appropriate free wake models (i.e. number of free wake turns, radial spacing of filaments, etc.) is a more challenging exercise with the IGE variant of the EHPIC code than with its OGE counterpart. The OGE problem is quite 'forgiving' in that the wake contraction is relatively gradual and consequently the relaxation solution can find the self-preserving wake geometry with little difficulty. However, the tightly spaced filaments characteristic of converged ground effect wakes represent a tougher challenge for the current solution method; though the algorithm is on the whole quite robust (as illustrated by the sample calculations described in the previous section), the code documentation in the User's Manual should be consulted when setting up IGE calculations.

The instructions in the User's Manual, along with the discussion of wake layout elsewhere in this report, should be helpful in guiding the user in the selection of such parameters as filament release point spacing and the number of free and prescribed wake turns for each filament. Also, it is important to note that the initial relaxation phase for IGE cases uses a stagnation point flow as an starting solution instead of the 'artificial climb' used in OGE calculations. In this new model a reduced value of the relaxation parameter CTINIT is appropriate; unlike the OGE case, where CTINIT should be chosen to be roughly twice the estimated final thrust coefficient for the run, CTINIT should set about equal to the estimated result multiplied by the ratio of the rotor height to the diameter. This coincides with the OGE rule-of-thumb at a height of two diameters, above which the rotor is effectively out of ground effect.

3.3 Performance Validation

A validation study was carried out as part of this effort, with data on several rotor systems drawn from References 12 and 13. Reference 12 featured a study of full scale rotor performance in flight for a wide variety of helicopters. A procedure was outlined by Hayden in Reference 12 to correct the rotor performance data for such effects as tail rotor power, main rotor profile power, and drive train losses in an attempt to extract the dependence of main rotor induced power on rotor height (the induced power was assumed to be the only component of the total power sensitive to height); this is an important preliminary to undertaking the validation exercise, since the EHPIC code is designed only to analyze isolated rotors (as opposed to complete, full-scale helicopters). Hayden began this correction process with the basic assumption that the power coefficient C_p is given by

$$C_p = C_{p_0} + KC_T^{3/2} \qquad (8)$$

The helicopter power data in Reference 12 consisted exclusively of measurements of in-flight shaft power for helicopters at various heights. Each aircraft displayed different curves of power vs. thrust at different heights; Hayden's approach was to extrapolate the available data to a zero-thrust condition, thus isolating the constant term in Equation 8, and then average the intercepts obtained for each rotor height. This averaged constant term was then removed from all power measurements to determine K for each height. He further assumed that a nondimensional rotor height of z/D = 2.0 represented a good approximation to out-of-ground-effect flight, so results for such cases were treated as the reference value K at infinity. Figure 12 shows the performance data plot for thirteen different helicopters (from Reference 12) as well as a curve fit through the data.

The data shown in Figure 12 was drawn from many different helicopters, including the AH-1, the OH-6, the UH-1, the H-55, and the OH-58, among others. For validation purposes, cases simulating both the two-bladed AH-1 rotor and the four-bladed OH-6 rotor were undertaken. In both cases, the rotor performance was computed at several different rotor heights from 0.4R to 2.0R. The results of these computations were adjusted and collapsed following the same procedure used in Reference 12.

The comparison shown in Figure 13 indicate that the prediction for the AH-1 case using the EHPIC code lies very close to the trend line computed by Hayden. The data for the AH-1 case itself displays some scatter around the computed trend line; it is also true that the behavior of the predictions (as well of the reduced data) can be sensitive to the exact manner in which curve fits are used to average the profile power contributions over the several different tests that contribute to the perfomance study. However, the performance predictions appear to agree well with the data to within the combined uncertainties of the original measurements and the corrections used to collapse the data.

The same conclusion is reached after inspection of Figure 14, which shows the K-factor as a function of rotor height for the four-bladed OH-6 helicopter. Once again the predictions fall near the trend line and the agreement can be considered good, especially in light of the relatively broad scatter evident in the original data presented in Figure 12. Still, the deviations of the predictions from the individual OH-6 data points are noticeably larger than in the AH-1 comparison above. It should be noted again that these plots compare predictions for isolated rotors to data from complete helicopters and that such direct comparisons are not strictly valid. The process used by Hayden to collapse a wide range of of dissimilar flight test data appears to be useful for evaluating broad trends, but it depends on several assumptions (e.g., the aggregation of fuselage and tail rotor effects into the constant term of Equation 8) that can produce unusual results in individual cases. Note that even small errors in the measured height of the rotor could substantially affect the correlation for the OH-6 in Figure 14. In such circumstances, the presence of the predictions within the scatter of the collapsed data is considered encouraging evidence of the capability of the modified EHPIC code to capture the major features of performance in ground effect. The shortcomings of this comparison only serve to emphasize the need to carry out a correlation study using data from a truly isolated rotor; this would permit a less ambiguous evaluation of the capabilities of the new version of EHPIC.

These results also point up some of the potential pitfalls of reliance on traditional simplified analyses of ground effect. An often-used approximation is to assume that profile

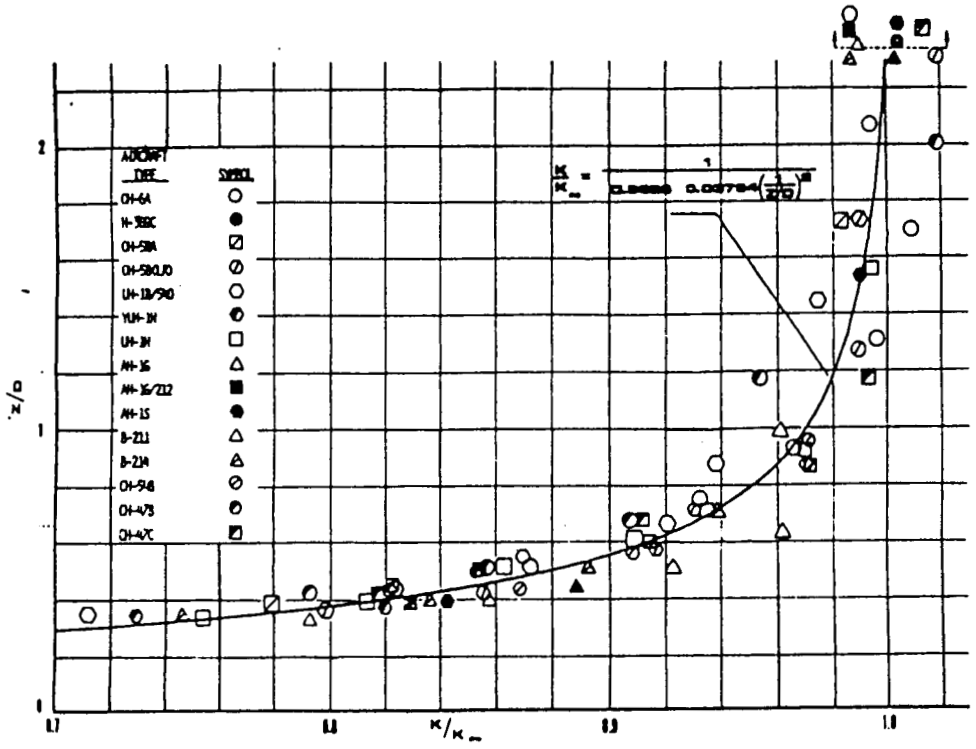

Figure 12. Data on ground effect on induced power required in hover (from Ref. 12).

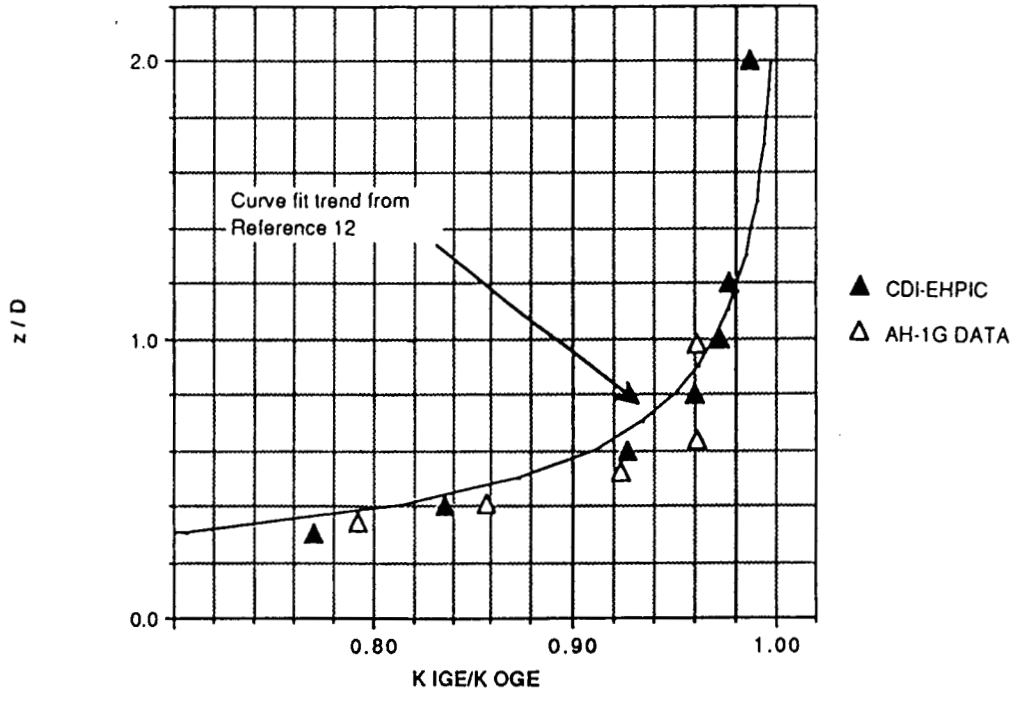

Figure.13. Predicted and measured performance in ground effect for the AH-1 rotor.

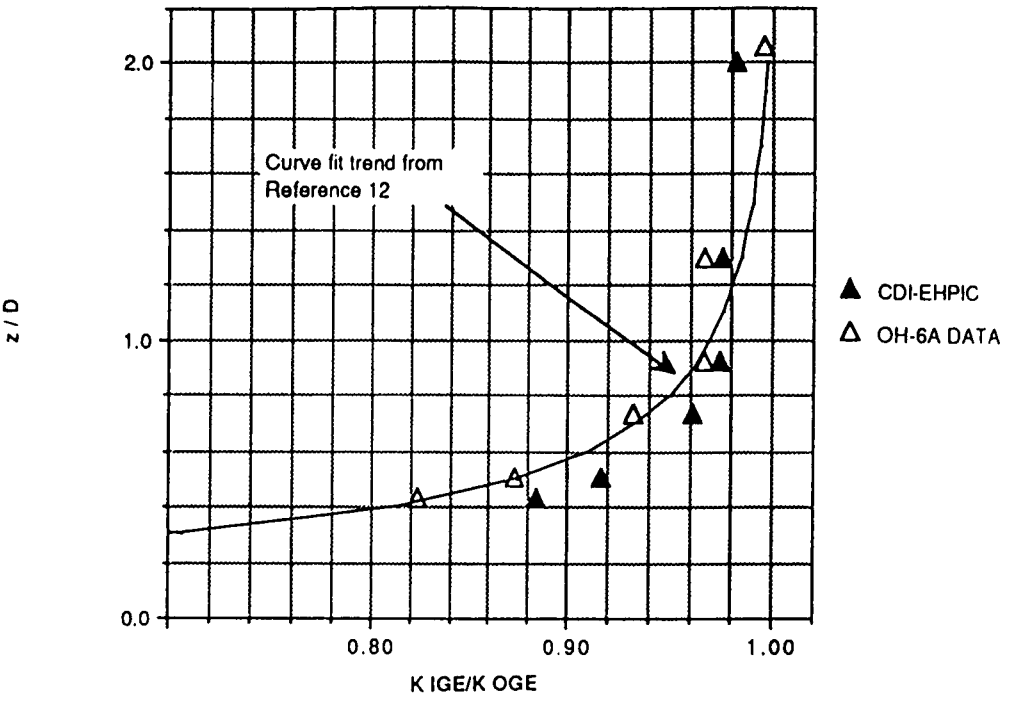

Figure 14. Predicted and measured performance in ground effect for the OH-6 rotor.

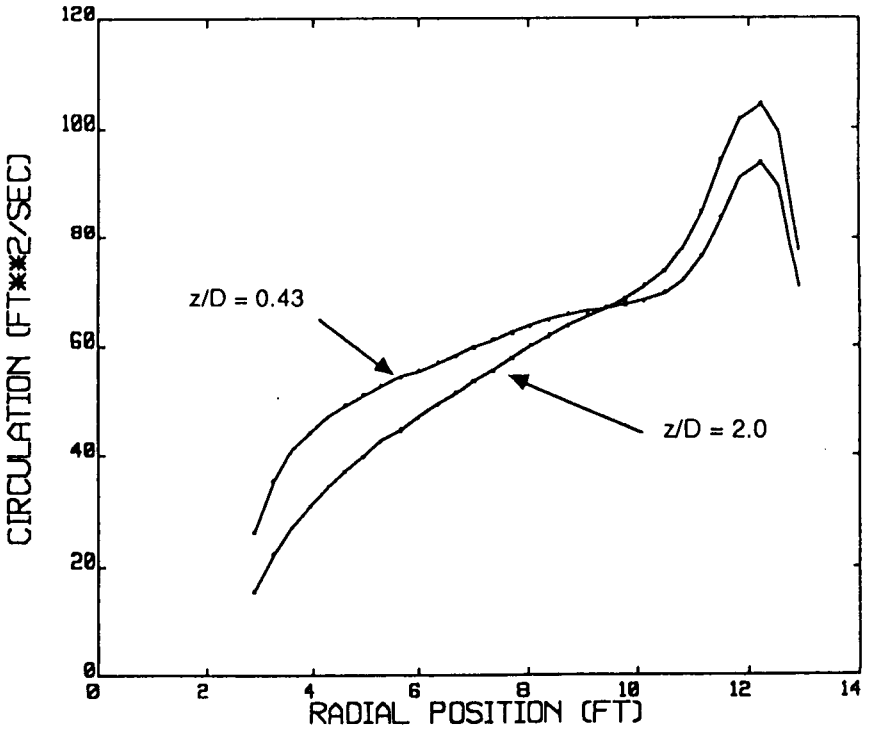

Figure 15. Bound circulation distribution comparison for the OH-6 rotor at z/D = .43 and 2.0 . (C_T constant at 0.0046)

power for a given thrust is independent of rotor height and to estimate IGE performance only on the basis of a modified value of induced power, usually arrived at by invoking a curve fit from empirical data like that derived by Hayden. The scatter noted in the supporting data (evident in Fig. 12) indicates that such an easy division of functional dependence in ground effect is an uncertain proposition. Also, Figure 15 shows the change in bound circulation distribution for specified thrust for the OH-6 at two different rotor heights. The substantial difference in load distribution indicates that the assumption of insensitivity of profile power to rotor height may be questionable, since the drag on the rotor will change as the local lift coefficients change. In this particular case, the computed profile power was five percent lower at z/D=0.430 than it was at z/D=2.0 (the thrust coefficient here was constant at 0.00462). This translates to a reduction of roughly one percent in total power, which is small compared to the twelve percent drop in induced power (a nine percent decrease in total power) but which may be significant in some cases. However, even the limited comparisons carried out here indicate that these trends may be configuration-dependent. For example, the two-bladed AH-1 rotor experiences a much smaller decrease in computed profile power as it enters ground effect, dropping only roughly one percent between z/D=2.0 and z/D=0.4 at a constant thrust coefficient of 0.0039. The overall message conveyed by these results is that though the assumption of the invariance of profile power with rotor height may be appropriate in many cases, significant dependence can exist and such an effect may need to be considered in situations where high accuracy is desired.

As a final example, several calculations were undertaken with more modern rotor designs, such as the three-bladed Advanced Technology Blade (ATB) variant of the XV-15 rotor. This rotor features highly twisted and tapered blades; calculations discussed in Reference 6 indicated that refined wake models were required to obtain accurate performance predictions for this design. It was of interest, therefore, to test whether or not the IGE variant of EHPIC could successfully converge the type of refined, multi-filament free wake that was used in the OGE calculations in Reference 6. Figure 16 shows the result of a typical ATB calculation using a six-filament free wake with the rotor operating at a thrust coefficient of 0.011 and at z/D = 1.0. The smooth convergence of the wake geometry is evident in this case; similar results have been obtained for other ATB runs. No ground effect performance data was available for systematic validation of the ATB runs, but the rotor figure of merit increased by two points (0.02) over its OGE value for this operating condition, so the correct qualitative trend was achieved. This sample calculation provided encouraging evidence of the ability of the IGE EHPIC code to produce results analogous to the successful OGE hover runs documented in References 5 and 6.

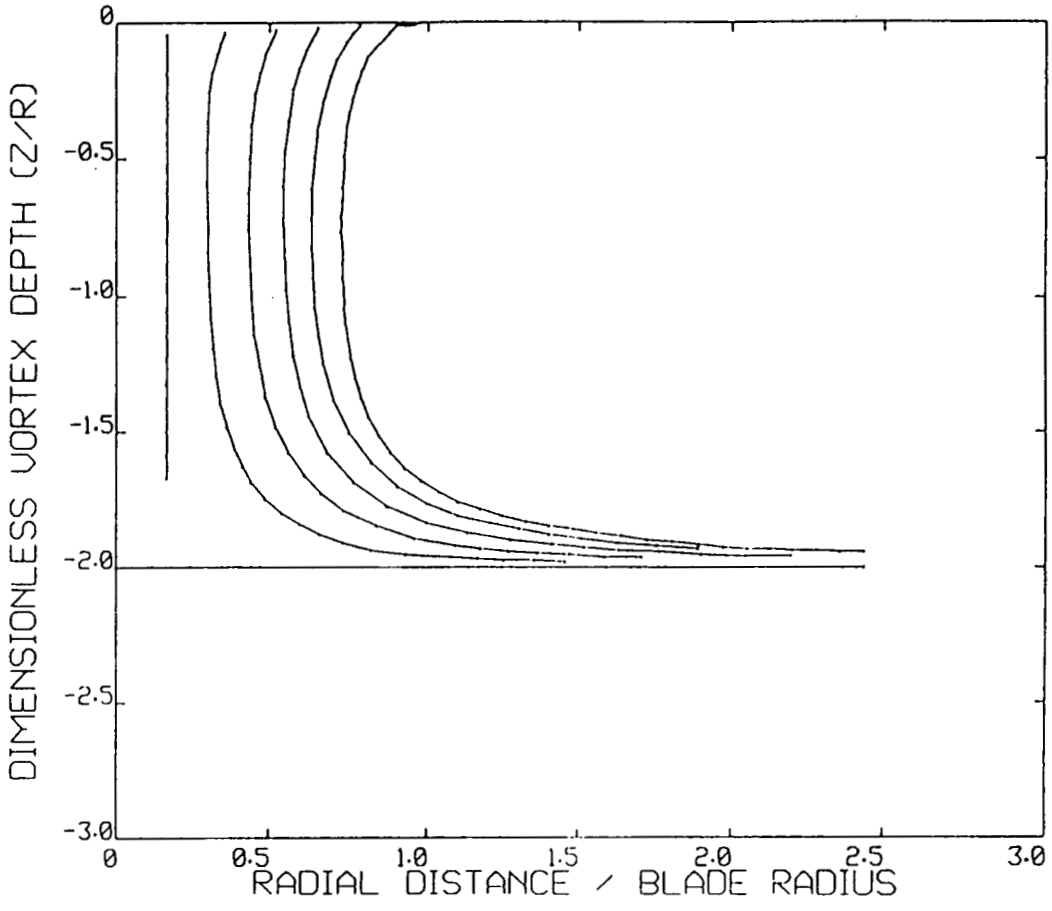

Figure 16. Wake geometry for the ATB rotor operating at $C_T = .011$.

4. WAKE STABILITY ANALYSIS

During the relaxation process, the matrix of influence coefficients is continuously updated. The final configuration of the matrix relates perturbations in the collocation point positions and the blade bound circulation to changes in the crossflow velocities in the wake and the downwash velocities at the blade control points. This relationship can be expressed as:

$$\begin{bmatrix} \Delta\vec{q} \\ \Delta\vec{w} \end{bmatrix} = \begin{bmatrix} Q_{qx} Q_{q\gamma} \\ Q_{wx} Q_{w\gamma} \end{bmatrix} \begin{bmatrix} \Delta\vec{x} \\ \Delta\vec{\gamma} \end{bmatrix} \tag{9}$$

This represents a set of coupled, linear differential equations for the crossflow and downwash velocities. The solution for these time-dependent velocities can be expressed as a linear combination of the eigenvectors of the influence coefficient matrix, with each vector multiplied by an exponential term whose argument is the associated eigenvalue. Since the eigenvalues are in general complex numbers, any eigenvalues with positive real parts indicate the presence of unstable modes in the computation for the crossflow and downwash velocities. Thus, examination of the eigenvalues yields significant information about the stability of the wake to small perturbations.

The updated documentation of the new version of the EHPIC code contains the detailed information necessary to invoke this stability analysis. The actual computation of the eigenvalues and eigenvectors is carried out using standard routines for real-valued arrays from the International Mathematical Subroutine Library (IMSL). Though a thorough analysis of the significance and interpretation of the wake stability information generated using this new capability is beyond the scope of this report, a limited discussion of representative cases and results is helpful for illustrating the usefulness and importance of this topic. Given the many different wake models that can be invoked using the EHPIC code (i.e. different numbers of filaments, blades, thrust levels, etc.), it would be difficult to compile a truly exhaustive set of results to cover all cases of interest in rotor wake aerodynamics. Consequently, the discussion below will focus on exploring relatively simple sample problems and on illustrating how the stability of various modes of motion in the wake are affected by the circulation strength of the trailing filaments (i.e. the rotor thrust), the rotor rotation frequency, and the extent of free wake used.

The first set of cases feature a simple one-bladed rotor with constant chord operating OGE; for this set of results, a single tip filament will be used and the blade will be modeled very coarsely using ten vortex quadrilaterals spanwise and one chordwise. Unless otherwise specified, the wake filament models employ eight 45 deg. arcs per turn of wake in the free wake region; the precribed wake model uses three turns of wake. Tables 1 and 2 present the eigenvalues obtained for two cases: first, a case using two turns of free wake and, second, a case with six turns of free wake. In both cases, the eigenvalues are a mix of real and complex values with, for the most part, negative real parts, indicating a large preponderance of stable modes. However, note the presence in both cases of eigenvalues with positive real parts, which are responsible for the nonconvergent behavior seen in previous time-marching calculations.

TABLE 1: Eigenvalues for a one-bladed sample rotor with two turns of free wake (thrust coefficient 0.0025).

Real part	Imag. part
-3.917E+02	0.000E+00
-1.245E+02	2.828E+01
-1.245E+02	-2.828E+01
-1.266E+02	1.310E+01
-1.266E+02	-1.310E+01
-1.195E+02	0.000E+00
-1.109E+02	4.741E+01
-1.109E+02	-4.741E+01
-9.557E+01	4.323E+01
-9.557E+01	-4.323E+01
-8.905E+01	5.820E+01
-8.905E+01	-5.820E+01
-8.183E+01	6.132E+01
-8.183E+01	-6.132E+01
-5.753E+01	6.898E+01
-5.753E+01	-6.898E+01
-4.803E+01	4.943E+01
-4.803E+01	-4.943E+01
-3.476E+01	5.349E+01
-3.476E+01	-5.349E+01
-4.128E+01	5.555E+01
-4.128E+01	-5.555E+01
-1.465E+01	4.736E+01
-1.465E+01	-4.736E+01
-1.564E+01	3.113E+01
-1.564E+01	-3.113E+01
-8.370E+00	2.426E+01
-8.370E+00	-2.426E+01
3.226E-01	1.430E+01
3.226E-01	-1.430E+01
-1.918E+01	1.753E+01
-1.918E+01	-1.753E+01
-5.221E+00	0.000E+00
-3.876E-01	0.000E+00
-4.169E-01	0.000E+00
-5.331E-01	0.000E+00
-6.102E-01	0.000E+00
-7.617E-01	0.000E+00
-8.274E-01	0.000E+00
-8.714E-01	0.000E+00
-9.111E-01	0.000E+00
-7.020E-01	0.000E+00
-9.338E-01	0.000E+00

TABLE 2: Eigenvalues for a one-bladed sample rotor with six turns of free wake (thrust coefficient 0.0025).

Real part	Imag. part
-3.918E+02	0.000E+00
-1.421E+02	4.702E+00
-1.421E+02	-4.702E+00
-1.377E+02	1.377E+01
-1.377E+02	-1.377E+01
-1.337E+02	0.000E+00
-1.364E+02	1.835E+01
-1.364E+02	-1.835E+01
-1.348E+02	2.500E+01
-1.348E+02	-2.500E+01
-1.323E+02	2.973E+01
-1.323E+02	-2.973E+01
-1.301E+02	3.555E+01
-1.301E+02	-3.555E+01
-1.257E+02	3.938E+01
-1.257E+02	-3.938E+01
-1.235E+02	4.577E+01
-1.235E+02	-4.577E+01
-1.172E+02	5.529E+01
-1.172E+02	-5.529E+01
-1.118E+02	6.307E+01
-1.118E+02	-6.307E+01
-1.165E+02	4.776E+01
-1.165E+02	-4.776E+01
-1.035E+02	6.525E+01
-1.035E+02	-6.525E+01
-1.007E+02	5.542E+01
-1.007E+02	-5.542E+01
-9.547E+01	6.709E+01
-9.547E+01	-6.709E+01
-9.122E+01	6.793E+01
-9.122E+01	-6.793E+01
-8.519E+01	7.122E+01
-8.519E+01	-7.122E+01
-8.087E+01	6.915E+01
-8.087E+01	-6.915E+01
-7.307E+01	7.426E+01
-7.307E+01	-7.426E+01
-6.216E+01	7.614E+01
-6.216E+01	-7.614E+01
-7.000E+01	6.834E+01
-7.000E+01	-6.834E+01
-5.314E+01	7.647E+01
-5.314E+01	-7.647E+01
-4.685E+01	7.550E+01
-4.685E+01	-7.550E+01
-5.802E+01	6.573E+01
-5.802E+01	-6.573E+01
-4.171E+01	6.778E+01
-4.171E+01	-6.778E+01
-3.627E+01	6.482E+01
-3.627E+01	-6.482E+01
-4.235E+01	5.665E+01
-4.235E+01	-5.665E+01
-3.629E+01	5.969E+01
-3.629E+01	-5.969E+01
-2.604E+01	6.091E+01
-2.604E+01	-6.091E+01
-1.734E+01	5.662E+01
-1.734E+01	-5.662E+01
-1.131E+01	5.200E+01
-1.131E+01	-5.200E+01
-3.105E+01	5.227E+01
-3.105E+01	-5.227E+01
-7.902E+00	4.720E+01
-7.902E+00	-4.720E+01
-2.515E+01	4.528E+01
-2.515E+01	-4.528E+01
-7.521E+00	4.252E+01
-7.521E+00	-4.252E+01
-1.837E+01	3.808E+01
-1.837E+01	-3.808E+01
-8.976E+00	3.296E+01
-8.976E+00	-3.296E+01
-7.096E+00	2.954E+01
-7.096E+00	-2.954E+01
-1.318E+01	2.764E+01
-1.318E+01	-2.764E+01
-7.112E-01	2.365E+01
-7.112E-01	-2.365E+01
2.533E+00	1.908E+01
2.533E+00	-1.908E+01
-1.414E+01	2.322E+01
-1.414E+01	-2.322E+01
3.761E+00	1.511E+01
3.761E+00	-1.511E+01
3.168E+00	1.152E+01
3.168E+00	-1.152E+01
-1.318E+01	1.640E+01
-1.318E+01	-1.640E+01
1.056E+00	7.923E+00
1.056E+00	-7.923E+00
-1.138E+01	9.719E+00
-1.138E+01	-9.719E+00
-7.837E+00	3.422E+00
-7.837E+00	-3.422E+00
-2.627E+00	0.000E+00
-3.758E-01	0.000E+00
-4.316E-01	0.000E+00
-5.329E-01	0.000E+00
-6.143E-01	0.000E+00
-7.011E-01	0.000E+00
-7.644E-01	0.000E+00
-9.339E-01	0.000E+00
-8.249E-01	0.000E+00
-8.702E-01	0.000E+00
-9.115E-01	0.000E+00

In the case with two free turns, though, there is a single unstable mode, while four unstable modes are evident in the case with six free turns. This trend to a higher number of unstable modes with an increasing extent of free wake continues for higher numbers of free turns (note, too, that the strength of the trailing tip vortices were kept the same in these two cases). It is also interesting to note that the unstable modes appear at relatively low frequency (fractions of the blade rotation frequency of 30 rad./sec.), indicating that these unstable modes correspond to relatively long wavelength disturbances. The analytical work in Reference 14 identified such long wavelength disturbances as one of the principal modes of instability in an infinite vortex helix.

Increasing the number of blades to four in the two cases just described produces the results shown in Tables 3 and 4. Note that additional unstable modes have arisen in each case. This corresponds qualitatively to the result found in Reference 15, where it was noted that increasing the number of interdigitated filaments in a set of infinite vortex helices brought about a broader spectrum of unstable eigenfrequencies. Direct comparisons between these numerical results and the analytical treatment of Reference 15 must, of course, be done cautiously since the computations here deal with a considerably different system with a finite number of degrees of freedom. Nonetheless, this correlation of behavior is expected and encouraging.

To explore the effect of increasing the circulation strength on these results, each of the cases discussed above was run at higher collective pitch; the results indicated only very slight changes in the eigenvalues. This confirmed the finding of Reference 16, which noted that the magnitude of the eigenvalues should scale not with the tip filament circulation Γ but with Γ/h_f^2, where h_f is a measure of the vertical spacing of the turns in the wake. This quantity can in turn be shown to be roughly proportional to the rotational frequency Ω (Ref. 16), and so the cases above were rerun at one-half the previous value of Ω. This calculation produced the results shown in Table 5 for the one-bladed rotor case and recovered the result of Reference 16 that indicated that the magnitude of the eigenvalues did in fact scale with Ω, as can be seen by comparing results with Table 2.

Using the wake stability analysis now present in the modified EHPIC code, many such parametric studies are possible. Among the prominent candidates are examination of multiple filament cases, possible suppression of instabilites in climb, the effect of ground proximity on unstable modes, and scrutiny of the eigenvectors associated with both stable and unstable modes to deduce the influence of the instabilites on the flow field around the rotor.

TABLE 3: Eigenvalues for a four-bladed sample rotor with two turns of free wake (thrust coefficient 0.0065).

Real part	Imag. part
-3.935E+02	0.000E+00
-1.272E+02	1.235E+01
-1.272E+02	-1.235E+01
-1.126E+02	0.000E+00
-1.185E+02	3.247E+01
-1.185E+02	-3.247E+01
-1.049E+02	4.998E+01
-1.049E+02	-4.998E+01
-1.136E+02	4.050E+01
-1.136E+02	-4.050E+01
-9.638E+01	5.147E+01
-9.638E+01	-5.147E+01
-6.871E+01	6.210E+01
-6.871E+01	-6.210E+01
-8.104E+01	4.953E+01
-8.104E+01	-4.953E+01
-3.726E+01	6.656E+01
-3.726E+01	-6.656E+01
-1.219E+01	6.062E+01
-1.219E+01	-6.062E+01
3.017E+00	4.856E+01
3.017E+00	-4.856E+01
7.251E+00	3.488E+01
7.251E+00	-3.488E+01
-6.095E+01	4.062E+01
-6.095E+01	-4.062E+01
3.003E+00	2.174E+01
3.003E+00	-2.174E+01
-4.253E+01	2.566E+01
-4.253E+01	-2.566E+01
-2.470E+01	8.684E+00
-2.470E+01	-8.684E+00
-6.848E+00	0.000E+00
-4.115E-01	2.397E-02
-4.115E-01	-2.397E-02
-5.253E-01	0.000E+00
-5.928E-01	0.000E+00
-9.342E-01	0.000E+00
-9.149E-01	0.000E+00
-7.571E-01	0.000E+00
-8.285E-01	0.000E+00
-6.916E-01	0.000E+00
-8.743E-01	0.000E+00

TABLE 4: Eigenvalues for a four-bladed sample rotor with six turns of free wake (thrust coefficient 0.0065).

Real part	Imag. part	Real part	Imag. part
-3.936E+02	0.000E+00	2.037E+00	6.041E+01
-1.408E+02	4.373E+00	2.037E+00	-6.041E+01
-1.408E+02	-4.373E+00	-6.626E+01	5.854E+01
-1.393E+02	1.334E+01	-6.626E+01	-5.854E+01
-1.393E+02	-1.334E+01	7.030E+00	5.468E+01
-1.360E+02	0.000E+00	7.030E+00	-5.468E+01
-1.368E+02	2.486E+01	-5.859E+01	5.407E+01
-1.368E+02	-2.486E+01	-5.859E+01	-5.407E+01
-1.352E+02	1.679E+01	1.049E+01	4.858E+01
-1.352E+02	-1.679E+01	1.049E+01	-4.858E+01
-1.329E+02	3.629E+01	-5.160E+01	4.879E+01
-1.329E+02	-3.629E+01	-5.160E+01	-4.879E+01
-1.318E+02	2.966E+01	1.227E+01	4.246E+01
-1.318E+02	-2.966E+01	1.227E+01	-4.246E+01
-1.279E+02	4.561E+01	-4.522E+01	4.311E+01
-1.279E+02	-4.561E+01	-4.522E+01	-4.311E+01
-1.264E+02	4.046E+01	1.275E+01	3.672E+01
-1.264E+02	-4.046E+01	1.275E+01	-3.672E+01
-1.226E+02	5.242E+01	-3.925E+01	3.707E+01
-1.226E+02	-5.242E+01	-3.925E+01	-3.707E+01
-1.161E+02	5.834E+01	1.222E+01	3.113E+01
-1.161E+02	-5.834E+01	1.222E+01	-3.113E+01
-1.171E+02	5.022E+01	-3.385E+01	3.064E+01
-1.171E+02	-5.022E+01	-3.385E+01	-3.064E+01
-1.085E+02	6.228E+01	1.059E+01	2.566E+01
-1.085E+02	-6.228E+01	1.059E+01	-2.566E+01
-1.060E+02	5.778E+01	-2.928E+01	2.430E+01
-1.060E+02	-5.778E+01	-2.928E+01	-2.430E+01
-1.004E+02	6.487E+01	7.906E+00	2.045E+01
-1.004E+02	-6.487E+01	7.906E+00	-2.045E+01
-9.416E+01	6.417E+01	-2.492E+01	1.872E+01
-9.416E+01	-6.417E+01	-2.492E+01	-1.872E+01
-9.096E+01	6.542E+01	4.519E+00	1.562E+01
-9.096E+01	-6.542E+01	4.519E+00	-1.562E+01
-6.927E+01	7.346E+01	-2.001E+01	1.339E+01
-6.927E+01	-7.346E+01	-2.001E+01	-1.339E+01
-8.193E+01	6.905E+01	2.415E-01	1.139E+01
-8.193E+01	-6.905E+01	2.415E-01	-1.139E+01
-8.235E+01	6.435E+01	-1.475E+01	8.076E+00
-8.235E+01	-6.435E+01	-1.475E+01	-8.076E+00
-5.645E+01	7.605E+01	-8.883E+00	3.175E+00
-5.645E+01	-7.605E+01	-8.883E+00	-3.175E+00
-4.408E+01	7.682E+01	-3.693E+00	0.000E+00
-4.408E+01	-7.682E+01	-4.104E-01	2.779E-02
-3.253E+01	7.597E+01	-4.104E-01	-2.779E-02
-3.253E+01	-7.597E+01	-5.202E-01	0.000E+00
-7.436E+01	6.186E+01	-5.914E-01	0.000E+00
-7.436E+01	-6.186E+01	-7.573E-01	0.000E+00
-2.189E+01	7.383E+01	-8.757E-01	0.000E+00
-2.189E+01	-7.383E+01	-8.276E-01	0.000E+00
-1.242E+01	7.025E+01	-9.146E-01	0.000E+00
-1.242E+01	-7.025E+01	-6.880E-01	0.000E+00
-4.422E+00	6.570E+01	-9.346E-01	0.000E+00
-4.422E+00	-6.570E+01		

TABLE 5: Eigenvalues for a one-bladed sample rotor with six turns of free wake (thrust coefficient 0.0025); rotor rotation rate reduced by 50% compared to Table 2.

Real part	Imag. part	Real part	Imag. part
-1.948E+02	0.000E+00	-1.333E+01	3.077E+01
-7.131E+01	2.418E+00	-1.333E+01	-3.077E+01
-7.131E+01	-2.418E+00	-1.823E+01	2.940E+01
-6.725E+01	1.219E+01	-1.823E+01	-2.940E+01
-6.725E+01	-1.219E+01	-8.938E+00	2.860E+01
-6.606E+01	0.000E+00	-8.938E+00	-2.860E+01
-6.895E+01	7.400E+00	-5.847E+00	2.627E+01
-6.895E+01	-7.400E+00	-5.847E+00	-2.627E+01
-6.718E+01	7.910E+00	-1.551E+01	2.585E+01
-6.718E+01	-7.910E+00	-1.551E+01	-2.585E+01
-6.559E+01	1.453E+01	-4.108E+00	2.387E+01
-6.559E+01	-1.453E+01	-4.108E+00	-2.387E+01
-6.503E+01	1.761E+01	-1.259E+01	2.237E+01
-6.503E+01	-1.761E+01	-1.259E+01	-2.237E+01
-6.217E+01	2.284E+01	-4.083E+00	2.137E+01
-6.217E+01	-2.284E+01	-4.083E+00	-2.137E+01
-6.227E+01	1.964E+01	-9.223E+00	1.885E+01
-6.227E+01	-1.964E+01	-9.223E+00	-1.885E+01
-5.936E+01	2.758E+01	-4.849E+00	1.654E+01
-5.936E+01	-2.758E+01	-4.849E+00	-1.654E+01
-5.640E+01	3.129E+01	-3.533E+00	1.486E+01
-5.640E+01	-3.129E+01	-3.533E+00	-1.486E+01
-5.726E+01	2.373E+01	-6.551E+00	1.362E+01
-5.726E+01	-2.373E+01	-6.551E+00	-1.362E+01
-5.193E+01	3.262E+01	-5.347E-01	1.181E+01
-5.193E+01	-3.262E+01	-5.347E-01	-1.181E+01
-4.998E+01	2.779E+01	-7.440E+00	1.127E+01
-4.998E+01	-2.779E+01	-7.440E+00	-1.127E+01
-4.745E+01	3.299E+01	1.165E+00	9.570E+00
-4.745E+01	-3.299E+01	1.165E+00	-9.570E+00
-4.507E+01	3.331E+01	1.810E+00	7.634E+00
-4.507E+01	-3.331E+01	1.810E+00	-7.634E+00
-4.280E+01	3.539E+01	-6.910E+00	8.132E+00
-4.280E+01	-3.539E+01	-6.910E+00	-8.132E+00
-3.712E+01	3.731E+01	1.514E+00	5.913E+00
-3.712E+01	-3.731E+01	1.514E+00	-5.913E+00
-4.011E+01	3.374E+01	-5.937E+00	4.815E+00
-4.011E+01	-3.374E+01	-5.937E+00	-4.815E+00
-3.173E+01	3.834E+01	4.325E-01	4.303E+00
-3.173E+01	-3.834E+01	4.325E-01	-4.303E+00
-2.717E+01	3.854E+01	-4.057E+00	1.710E+00
-2.717E+01	-3.854E+01	-4.057E+00	-1.710E+00
-3.486E+01	3.322E+01	-1.509E+00	0.000E+00
-3.486E+01	-3.322E+01	-2.210E-01	0.000E+00
-2.392E+01	3.770E+01	-3.039E-01	0.000E+00
-2.392E+01	-3.770E+01	-4.139E-01	0.000E+00
-2.908E+01	3.209E+01	-5.053E-01	0.000E+00
-2.908E+01	-3.209E+01	-5.994E-01	0.000E+00
-2.122E+01	3.378E+01	-7.498E-01	0.000E+00
-2.122E+01	-3.378E+01	-8.057E-01	0.000E+00
-1.823E+01	3.238E+01	-8.487E-01	0.000E+00
-1.823E+01	-3.238E+01	-6.764E-01	0.000E+00
-2.174E+01	2.858E+01		
-2.174E+01	-2.858E+01		

5. CPU TIME REDUCTION VIA VECTORIZATION

Major modfications were made to the original version of the EHPIC code (denoted MOD 0.0) for the purpose of optimizing it for execution on the CRAY X-MP vector processing computer. The optimization procedure for the EHPIC code involved,

a) locating the subroutines where most of the calculation time takes place,

b) restructuring these subroutines in order to take advantage of vector processing, and,

c) restructuring sections of these subroutines in order to take advantage of certain scalar processing features of the CRAY X-MP.

When operating in vector mode, the modified EHPIC code (denoted MOD 1.0) typically runs between 4.0 and 4.7 times faster than the original EHPIC code (MOD 0.0) operating in scalar mode.

5.1 Locating the CPU Time

Timings were made on the CDI's in-house MicroVax II for the sample job found in the Users Manual and for a more time-consuming run in ground effect. The results revealed that the vast majority of the processor time was spent performing Biot-Savart velocity induction calculations. Most of the CPU time was spent in calculating the wake-on-wake and wake-on-blade effects in subroutine HCPAR. However, runs with several blades and/or a dense layout of vortex quadrilaterals on the blade did require a significant amount of time in the performance evaluation subroutine HCPERF. The blade-on-wake effect calculated in subroutine HCBOW and the matrix inversion performed in subroutine HCSOL account for virtually all of the remaining calculation time. The timing breakdown for the sample job and the ground effect job run on the MicroVax II were found to be:

CPU Time (in seconds) for Timed Jobs

SUBROUTINE:	HCPAR	HCPERF	HCBOW	HCSOL
SAMPLE Job:	70%	19%	5%	6%
GRND EFFCT Job:	88%	5%	3%	4%

The sample job is a good example of a run where the number of blade control points is nearly the same as the number of wake points. This results in a larger percentage of the total calculation time being spent in HCPERF. The ground effect job is a good example of a wake-dominated run; these runs are usually more time consuming and almost all the time is spent performing the wake induced velocity calculations in HCPAR.

5.2 Restructuring for Vector Processors

The next step in the code modification involved restructuring the CPU-intensive routines so that they would run in vector mode. Background information of general vector processing techniques is contained in Reference 17. The following discussion often alludes to information found in this reference.

On the CRAY, vector processing is approximately ten times faster than scalar processing. Vector processors save time by performing the lines of eligible DO loops simultaneously when possible. In general, eligible DO loops CANNOT contain

a) other do loops,

b) subroutine calls, or

c) branches (IF THEN ELSE/GO TO statements).

There are other criteria, but these pose the major obstacles when modifying a code that was originally written for a scalar processor.

The DO loops that account for most of the CPU time are the ones that are targeted for vector mode. Not only are subroutine calls and branches removed from these DO loops, but the code is also restructured to maximize their limits; the higher the loop limit, the greater the gain from the vector processing. Although it would appear from the previous section that only four subroutines needed to be modified for optimization, this is not the case. The EHPIC code is highly modularized. HCPAR, for example, calls several other subroutines which in turn call still more. A large scale restructuring of the EHPIC code was required in order to allow vectorization of the time intensive routines. The changes are documented in the code and the MOD 1.0 Program Maintenance Manual.

The basic task of the restructuring was to store the necessary information needed for all the velocity induction calculations required for each BCVE (and blade quadrilateral) before entering the associated vectorized DO loop that performs the calculations. A few major obstacles had to be addressed:

1. The analytical representation of the Biot-Savart integral in the velocity induction calculation takes on two different forms depending on the sign of one of the variables. (See Reference 7, Appendix A). This branch is intrinsic to the current algorithm and could not be removed. Calculations involving each form had to be grouped together and solved separately.

2. The current core model is only invoked when the point of evaluation is in the vicinity of the BCVE that is inducing the velocity. Removing this branch would require altering the current core model. Therefore, all calculations at points within a certain region (the subinterval region discussed in Section 2.1.1 of Reference 7) are grouped together and are performed in scalar mode. These typically account for less than 10% of the total number of BCVE calculations.

3. The algorithm for the analytic summation of far wake induced velocity must be performed in scalar mode because it contains some iterative procedures. However, the far wake summation accounts for only a small percentage of the total calculation time and is not even present in the more time-consuming ground effect runs.

Further details concerning the restructuring of the code can be found within the code and the Mod 1.0 Program Maintenance Manual.

5.3 Results of Scalar and Vector Optimization on the CRAY X-MP

The Cray X-MP has 12 functional units and the ability to perform two FETCHES and one STORE per each CHAINED command (see Reference 17). It also performs multiplications more than three times faster than divisions in both scalar and vector mode. The most time-intensive routines were optimized based on this information resulting in a 40% increase in efficiency on the Cray X-MP before vectorization.

The results of the code optimization are shown in the Figures 17 and 18 for the two jobs previously discussed. On the CRAY X-MP, the sample job (a two bladed rotor with four free filaments) ran 4.0 times faster with EHPIC MOD 1.0 in vector mode than with EHPIC MOD 0.0 in scalar mode. The ground effect job, which featured a four-bladed rotor with four free filaments, ran 4.7 times faster. These results should be representative of a broad range of EHPIC runs.

To gauge the extent to which the potential for CPU time reduction via vectorization has been fulfilled, it is helpful to consult Amdahl's Law, which states that if vector operations are performed ten times faster than scalar operations, then

$$Fv = 1.11(1 - 1/P) \tag{10}$$

where Fv is the fraction of operations performed in vector mode and P is the total performance, or the number of operations performed per unit time (scaled so that P = 1 corresponds to scalar mode). The vector optimization accounts for a factor of roughly 2.5 to 3.0 increase in total performance, which means that roughly 70% of the operations are currently being performed in vector mode. The following timings were made on the CRAY X-MP for EHPIC MOD 1.0 operating in vector mode.

CPU Time (in seconds) for Timed Jobs

SUBROUTINE:	HCPAR	HCPERF	HCBOW	HCSOL
SAMPLE Job:	72%	18%	4%	4%
GRND EFFCT Job:	92%	1%	2%	3%

Since these routines have all been vectorized and they still account for 98% of the computation time, little more can be done in terms of vector optimization.

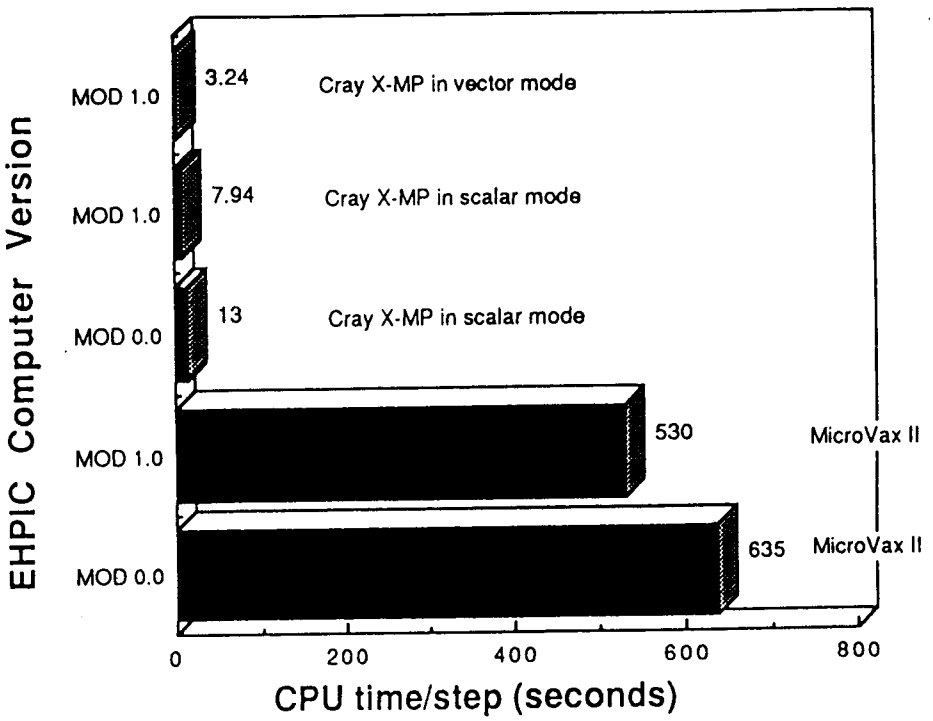

Figure 17. Run time comparisons for original and modified versions of the EHPIC code: two-bladed sample rotor OGE.

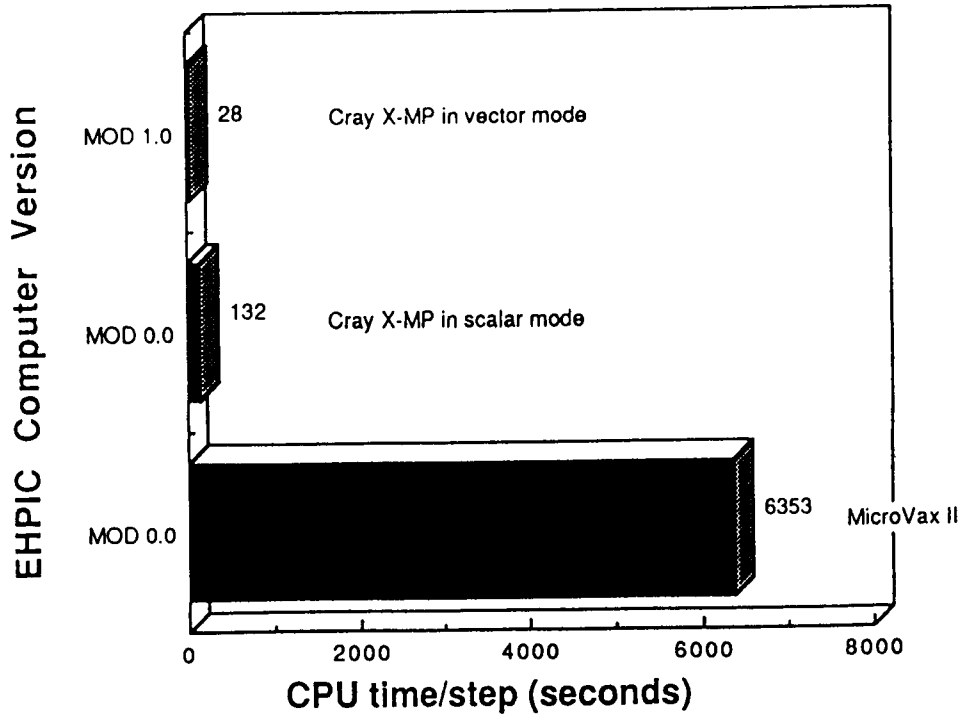

Figure 18. Run time comparisons for original and modified versions of the EHPIC code: four-bladed OH-6 rotor IGE.

6. CONCLUSION

This report has summarized the results of three distinct efforts whose common goal was to enhance the applicability and utility of the EHPIC free wake hover performance prediction program. The primary task in this three-part effort revolved around the addition of an image wake to the original version of the EHPIC analysis to permit exploration of the effect of ground proximity on rotor performance. Representative calculations were carried out to test the adequacy of the current ground effect model and the comparisons obtained with existing full-scale helicopter performance data were encouraging. Further validation efforts would be desirable, though, in particular comparisons with isolated rotor data. Also, further research on the treatment of the prescribed wake and the far wake should be carried out to make the ground effect variant of the analysis easier to operate reliably.

In particular, the rules of thumb outlined above for the selection of the extent of free wake assigned to each of the free filaments trailed from the blade must be firmed up and generalized. In OGE cases, it was usually found that selecting a tip vortex with somewhat less than twice the number of free turns as the free inboard vortices allows all the free filaments to terminate at approximately the same axial distance below the disk, a circumstance that is desirable for smooth and reliable convergence. Analogous criteria that lead to well-behaved solutions are still being evolved for cases in ground effect; the addition of the rotor height as a new "degree of freedom" complicates the specification of widely applicable rules, but the approach of using a free turn ratio of at least 2:1 (tip:inboard) enjoyed considerable success in the runs performed here (though, as discussed above, higher ratios are sometimes required for runs very near the ground). Observing this rule while taking the tip vortex out to a radial distance at least equal to the rotor height (and in no case less than one rotor diameter) has usually proved to be a satisfactory approach in the calculations executed to date. In fact, terminating the tip vortex wake still farther out is preferable; truncating the wake at two diameters is a conservative approach. To accelerate the "learning curve" that is inevitably encountered with new capabilities like the IGE option, additional calculations are being performed to confirm and extend these rules of thumb.

The second task undertaken here involved exploiting a capability that has been latent in the influence coefficient solution method since the original work on this topic documented in Reference 16. It is now possible to undertake wake stability analyses for converged solutions using the eigensystem analysis from the IMSL library described in Section 4. The sample calculations shown there are only illustrations of the many possible applications of this capability, though they do indicate that the linearized stability analysis represented by these eigenvalue calculations predicts trends consistent with previous analytical and computational work on stability of vortex helices.

Finally, the EHPIC code has been extensively rewritten to take advantage of the vector processing capabilities of CRAY-type supercomputers. Runs on the NASA CRAY X-MP have shown that the modified version of the EHPIC code should run four to five times faster than the original version designed for serial processing machines. This enhancement of efficiency is clearly important in any application of the EHPIC code, but particularly so in light of the increased CPU time required by the new ground effect model described above.

REFERENCES:

1. Bliss, D. B., Wachspress, D.A., and Quackenbush, T.R.: "A New Approach to the Free Wake Problem for Hovering Rotors," Proceedings of the 41st Annual Forum of the American Helicopter Society, May 1985.

2. Quackenbush, T.R., Bliss, D.B., Wachspress, D. A., and Ong, C.C.: "Free Wake Analysis of Hover Performance Using a New Influence Coefficient Method," NASA CR 4150, 1988.

3. Landgrebe, A.J.: "An Analytical and Experimental Investigation of Helicopter Rotor Hover Performance and Wake Geometry Characteristics," USAAMRDL TR 71-24, June 1971.

4. Scully, M.P.: "Computation of Helicopter Rotor Wake Geometry and Its Influence on Rotor Harmonic Airloads," M.I.T., ASRL TR 178-1, March 1975.

5. Quackenbush, T.R., Bliss, D.B., and Wachspress, D.A.: "Computational Analysis of Hover Performance Using a New Free Wake Method," Proceedings of the Second International Conference of Rotorcraft Basic Research, College Park, MD, February 1988.

6. Felker, F.F., Quackenbush, T. R., Bliss, D.B., and Light, J.L.: "Comparisons of Predicted and Measured Rotor Performance Using a New Free Wake Method," Proceedings of the 44th Annual Forum of the AHS, June 1988.

7. Bliss, D. B., Teske, M.E., and Quackenbush, T.R.: "A New Methodology for Free Wake Analyses Using Curved Vortex Elements," NASA CR 3958, 1986.

8. Taylor, M.K.: "A Balsa-Dust Technique for Air-Flow Visualization and Its Application to Flow Through Model Helicopter Rotors in Static Thrust," NACA TN 2220, 1950.

9. Heyson, H.H.: "An Evaluation of Linearized Vortex Theory as Applied to Single and Multiple Rotors Hovering In and Out of Ground Effect," NASA TN-D 43, 1959.

10. Fradenburgh, E.A.: "The Helicopter and the Ground Effect Machine," Journal of the American Helicopter Society, Vol. 5, No. 4, October 1960.

11. Piziali, R. and Felker, F.F.: "Reduction of Unsteady Recirculation in Hovering Model Helicopter Rotor Testing," Journal of the American Helicopter Society, Vol. 32, No. 1, January 1987.

12. Hayden, J.S.: "The Effect of the Ground on Hovering Power Required," Proceedings of the 32nd Annual Forum of the American Helicopter Society, May

13. Zborzek, J.: "Ground Effect on the Lifting Rotor," Great Britain Aeronautical Research Council, R&M 2347, July 1987.

14. Widnall, S.E., Tsai, C.-Y., and Bliss, D.B.: "The Instability of Short Waves on a Vortex Ring," J. Fluid Mech. 66 (1), October 1974.

15. Gupta, B.P. and Loewy, R. G.: "Theoretical Analysis of the Aerodynamic Stability of Multiple, Interdigitated Helical Vortices," AIAA Journal, Vol. 12, No. 10, October 1974.

16. Bliss, D.B., Wachspress, D.A., Quackenbush, T.R., and Bilanin, A.J.: "A New Approach to the Free Wake Problem for Hovering Rotors," Continuum Dynamics, Inc. Report No. 84-7, (Final Report to NASA Under Contract NAS2-11730), June

17. Levesque, J.M. and Williamson, J.: "Efficient FORTRAN Techniques for Vector Processors," Pacific-Sierra Research Corp., 1986.

1. Report No.	2. Government Accession No.	3. Recipient's Catalog No.
NASA CR-177523		

4. Title and Subtitle	5. Report Date
ENHANCEMENTS TO A NEW FREE WAKE HOVER ANALYSIS	April 1989
	6. Performing Organization Code

7. Author(s)	8. Performing Organization Report No.
Todd R. Quackenbush and Daniel A. Wachspress	
	10. Work Unit No. 505-61-51

9. Performing Organization Name and Address	11. Contract or Grant No.
Continuum Dynamics, Inc. P.O. Box 3073 Princeton, New Jersey 08540	NAS2-12810
	13. Type of Report and Period Covered
12. Sponsoring Agency Name and Address	Contractor Report
National Aeronautics and Space Administration Washington, DC 20546-0001	14. Sponsoring Agency Code

15. Supplementary Notes

Point of Contact: Jeffrey Light, MS T-031, Ames Research Center, Moffett Field, CA 94035 (415)694-4881 or FTS 464-4881

16. Abstract

This report summarizes the results of three distinct efforts whose common goal was to enhance the applicability and utility of the EHPIC (Evaluation of Hover Performance using Influence Coefficients) free wake hover performance prediction program. The primary task in this three-part effort revolved around the addition of an image wake to the original version of the EHPIC analysis to permit exploration of the effect of ground proximity on rotor performance. Representative calculations were carried out to test the adequacy of the current ground effect model and the comparisons obtained with existing full-scale helicopter performance data was encouraging. The second task undertaken here involved exploiting a capability that has been latent in the influence coefficient solution method since the original work on this topic. The modified EHPIC code can now undertake wake stability analyses for converged solutions using an existing eigensystem analysis package. Sample calculations are shown herein that illustrate some of the many possible applications of this capability. Finally, the EHPIC code has been extensively rewritten to take advantage of the vector processing capabilities of CRAY-type supercomputers. Test runs on the NASA CRAY X-MP have shown that the modified version of the EHPIC code runs four to five times faster than the original version designed for serial processing machines.

17. Key Words (Suggested by Author(s))	18. Distribution Statement
hover performance free wakes ground effect vectorization	Unclassified - Unlimited Subject Category: 02

19. Security Classif. (of this report)	20. Security Classif. (of this page)	21. No. of Pages	22. Price
Unclassified	Unclassified	41	A03

For sale by the National Technical Information Service, Springfield, Virginia 22161

1. Report No.	2. Government Accession No.	3. Recipient's Catalog No.
NASA CR-177523		

4. Title and Subtitle	5. Report Date
ENHANCEMENTS TO A NEW FREE WAKE HOVER ANALYSIS	April 1989
	6. Performing Organization Code

7. Author(s)	8. Performing Organization Report No.
Todd R. Quackenbush and Daniel A. Wachspress	
	10. Work Unit No. 505-61-51

9. Performing Organization Name and Address	11. Contract or Grant No.
Continuum Dynamics, Inc. P.O. Box 3073 Princeton, New Jersey 08540	NAS2-12810
	13. Type of Report and Period Covered
12. Sponsoring Agency Name and Address	Contractor Report
National Aeronautics and Space Administration Washington, DC 20546-0001	14. Sponsoring Agency Code

15. Supplementary Notes

Point of Contact: Jeffrey Light, MS T-031, Ames Research Center, Moffett Field, CA 94035 (415)694-4881 or FTS 464-4881

16. Abstract

~~This report summarizes~~ the results of three distinct efforts whose common goal was to enhance the applicability and utility of the EHPIC (Evaluation of Hover Performance using Influence Coefficients) free wake hover performance prediction program. ARE SUMMARIZED. The primary task in this three-part effort revolved around the addition of an image wake to the original version of the EHPIC analysis to permit exploration of the effect of ground proximity on rotor performance. Representative calculations were carried out to test the adequacy of the current ground effect model and the comparisons obtained with existing full-scale helicopter performance data was encouraging. The second task undertaken ~~here~~ involved exploiting a capability that has been latent in the influence coefficient solution method since the original work on this topic. The modified EHPIC code can now undertake wake stability analyses for converged solutions using an existing eigensystem analysis package. Sample calculations are shown ~~herein~~ that illustrate some of the many possible applications of this capability. Finally, the EHPIC code ~~has been~~ WAS extensively rewritten to take advantage of the vector processing capabilities of CRAY-type supercomputers. Test runs on the NASA CRAY X-MP have shown that the modified version of the EHPIC code runs four to five times faster than the original version designed for serial processing machines.

17. Key Words (Suggested by Author(s))	18. Distribution Statement
hover performance free wakes ground effect vectorization	Unclassified - Unlimited Subject Category: 02

19. Security Classif. (of this report)	20. Security Classif. (of this page)	21. No. of Pages	22. Price
Unclassified	Unclassified	41	A03

For sale by the National Technical Information Service, Springfield, Virginia 22161